LEVEL II

HDL-CR-78-025-1

October 1978

Effect of Angle of Attack on Cavity Flow Oscillations

by

V. Sarohia and P. F. Massier

Prepared by

Jet Propulsion Laboratory
California Institute of Technology
Pasadena, CA 91103
(JPL Publication 79-19)

Under contract
MIPR No. R-77-25

U.S. Army Electronics Research
and Development Command
Harry Diamond Laboratories
Adelphi, MD 20783

The findings in this report are not to be construed as an official Department of the Army position unless so designated by other authorized documents.

Citation of manufacturers' or trade names does not constitute an official indorsement or approval of the use thereof.

Destroy this report when it is no longer needed. Do not return it to the originator.

UNCLASSIFIED

SECURITY CLASSIFICATION OF THIS PAGE (When Data Entered)

REPORT DOCUMENTATION PAGE

READ INSTRUCTIONS BEFORE COMPLETING FORM

1. REPORT NUMBER: HDL-CR-78-025-1	2. GOVT ACCESSION NO.
	3. RECIPIENT'S CATALOG NUMBER
4. TITLE (and Subtitle): Effect of Angle of Attack on Cavity Flow Oscillations	5. TYPE OF REPORT & PERIOD COVERED: Final Report, Phase II
	6. PERFORMING ORG. REPORT NUMBER: JPL Publication 79-19
7. AUTHOR(s): V. Saronia and P. F. Massier	8. CONTRACT OR GRANT NUMBER(s): MIPR No. R-77-25
9. PERFORMING ORGANIZATION NAME AND ADDRESS: Jet Propulsion Laboratory, California Institute of Technology, Pasadena, CA 91103	10. PROGRAM ELEMENT, PROJECT, TASK AREA & WORK UNIT NUMBERS: Program Element: 6.21.14.A
11. CONTROLLING OFFICE NAME AND ADDRESS: Harry Diamond Laboratories, 2800 Powder Mill Road, Adelphi, MD 20783	12. REPORT DATE: October 1978
	13. NUMBER OF PAGES: 48
14. MONITORING AGENCY NAME & ADDRESS (if different from Controlling Office)	15. SECURITY CLASS. (of this report): UNCLASSIFIED
	15a. DECLASSIFICATION/DOWNGRADING SCHEDULE

16. DISTRIBUTION STATEMENT (of this Report)

Approved for public release; distribution unlimited

17. DISTRIBUTION STATEMENT (of the abstract entered in Block 20, if different from Report)

18. SUPPLEMENTARY NOTES

HDL Project No.: 304734
DA Code: 1L162114AH73
DRCMS Code: 612114.11.H7300

19. KEY WORDS (Continue on reverse side if necessary and identify by block number)

Jets, Wakes, and Viscid-Inviscid Flow Interactions

20. ABSTRACT (Continue on reverse side if necessary and identify by block number)

Separated subsonic flow over cavities of several widths and depths located on fuze-nose and ellipsoidal axisymmetric bodies have been investigated experimentally at various angles of attack to the free-stream. The fluctuating and mean velocities and pressures inside the cavity were measured at various circumferential locations. Large circumferential variations in the root mean square pressure fluctuations were observed in the cavity at an angle of attack. The hot-wire measurements of velocity fluctuations showed that the circumferential

DD FORM 1473, 1 JAN 73 EDITION OF 1 NOV 65 IS OBSOLETE

UNCLASSIFIED

SECURITY CLASSIFICATION OF THIS PAGE (When Data Entered)

291 250

20.

variations in cavity pressure oscillations were caused by the loss of spanwise coherency of the large-scale structures around the cavity. Visualization of the flow further confirmed that the strength of the cavity pressure fluctuations was closely related to the presence of the large-scale organized fluctuations in the cavity shear flow. The mean velocity measurements showed changes in growth rates, $d\theta/dx$, at various circumferential locations along the cavity shear layer, where θ is the momentum thickness, and x is the streamwise coordinate. High-speed Schlieren motion pictures further showed that this growth of the shear layer was accompanied by a process of the large-scale eddies engulfing the fluid inside the cavity. The engulfed fluid was subsequently carried by these eddies into the potential flow surrounding the cavity and remained unmixed downstream from the cavity for many wavelengths of the convecting large-scale eddies. For the fuze-nose model, the upstream edge of the axisymmetric cavity should be located at $X_0 \geq 1.25$ in. for cavity flow to oscillate. At this location, for cavity widths ≥ 0.25 in. and depths ≥ 0.050 in., the cavity flow oscillations were observed at free-stream velocities ≥ 500 ft/s.

CONTENTS

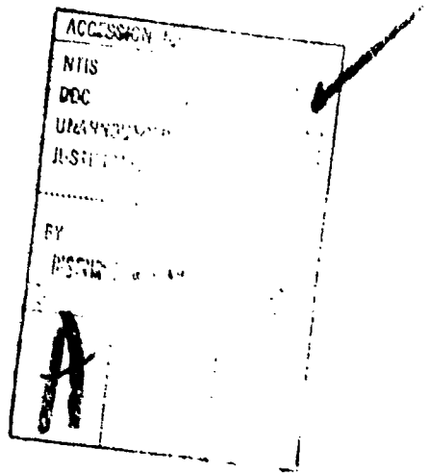

Tables

Effect of Angle of Attack on Pressure Oscillations Inside Cavity

Figures

1. INTRODUCTION

It has been observed by many investigators, e.g., East (Ref. 1), Karamcheti (Ref. 2), Roshko (Ref. 3), Sarohia (Ref. 4), that a separated shear layer over a cavity sustains oscillations over a wide range of Mach numbers and Reynolds numbers, with both laminar and turbulent boundary layers and over a wide range of length to depth ratios. Shadowgraph pictures of Sarohia and Massier (Ref. 5) indicate the presence of organized large-vortex structures in the oscillating flow over an axisymmetric cavity for both a laminar as well as a turbulent boundary layer at the upstream cavity corner. These pictures, along with detailed measurements taken in the cavity shear layer under a wide range of cavity configurations and flow conditions (Sarohia, Ref. 6), strongly indicate that the cavity flow oscillation phenomenon results primarily from the inherent instability of the mean velocity in the shear layer over the cavity. This instability results from the presence of an inflection point in the profile, which occurs for both laminar and turbulent separated flows over the cavity. Experimental results (Ref. 6) showed that the organized flow disturbances caused by these large-scale structures in the cavity shear layer are amplified almost exponentially as they propagate downstream. Due to the strong influence of the feedback from the downstream cavity corner, no merging or pairing of these organized structures with each other occurred in the cavity mixing layer. Such merging was observed, however, in free shear flows by Brown and Roshko (Ref. 7), Winant and Browand (Ref. 8), and others. The presence of the large organized structures in the flow contributed to a larger growth of the cavity shear layer than for a freely developing one. These large structures have been shown to be greatly responsible for the pressure fluctuations inside the cavity (Ref. 5).

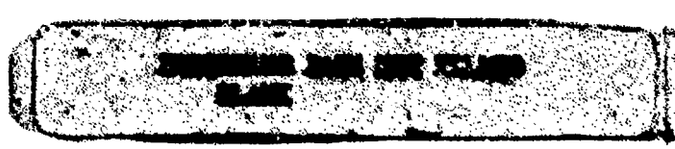

In Sarohia (Ref. 6), the signals detected by a reference hot-wire probe were cross correlated with those detected by a second probe which was moved circumferentially. These cross correlations showed that when the cavity was aligned with the free-stream flow, the flow oscillations were axisymmetric. The spark shadowgraphs of the cavity flow also showed that the large-scale structures associated with cavity flow oscillations were circumferentially coherent. Since these oscillations result from strong feedback with the downstream cavity corner, a comparatively large modification of this feedback behavior results. Consequently, the cavity-flow oscillations are modified when the free-stream velocity is at an angle of the attack with respect to the axis of the axisymmetric cavity. Knowledge of the manner in which the cavity flow is modified circumferentially at an angle of attack can lead to increased insight into the mechanism of these self-sustained oscillations.

Experimental results of Willmarth et al. (Ref. 9) showed that pressure oscillations inside an axisymmetric cavity were sensitive to the angle of the cavity with respect to the free-stream. Willmarth et al. reported that velocity and pressure flucutations, associated with cavity shear flow, varied largely as the angle of the free-stream was varied with respect to the axis of the cavity. Unfortunately, no detailed measurements of the flow field around the cavity were made to determine the basic modification of cavity flow associated with the angle of attack configuration.

The experiments conducted under the present investigation were performed to advance the understanding of the manner in which initial flow conditions at the upstream cavity corner influence the phenomenon of cavity flow oscillations. Flow visualization and detail measurements of cavity shear layer velocity and pressure measurement inside the cavity were made to help gain further insight

into the mechanism of oscillations in separated cavity flows. Due to the modification of the spanwise coherency of these organized large-scale structures in the cavity flow, these measurements have also elucidated the role of spanwise structures in the development of separated shear flows.

2. EXPERIMENTAL ARRANGEMENT

2.1 Model and Free-Jet Facility

The cavity model, as indicated in Figure 1, was mounted on a movable platform. This platform allowed the model to be positioned at various angles up to $\pm 10°$ with respect to the axis of the free jet. The model, which had a diameter D = 2.0 in., was tested in a 7-in.-diameter open-jet tunnel. A semicircular arc ring of 10-in. diameter, which was large enough not to disturb the free-jet flow, was constructed around the cavity model as shown in Figure 2. This ring carried a hot-wire probe which could be positioned at various circumferential locations around the cavity flow. The hot-wire probe could be moved accurately along the streamwise direction, x, and across the flow, y, at various selected circumferential locations with an accuracy of ± 0.001 in.

Two axisymmetric models were employed for this investigation. One had an ellipsoidal nose shape and the other had a fuze nose. Both models had provision for step variation of depth, d, together with a continuously adjustable width, b. The ellipsoidal-nose model was used primarily for flow visualization and for measurement of fluctuating and mean velocity components in the cavity shear layer. Most of the pressure measurements inside the cavity were made with the fuze-nose shape model as shown in Figure 1. A depth of 0.1 in. was selected for which the width was changed in steps having values of 0.3, 0.4, and 0.475 in. This model had provision for inserting a pressure transducer at the base of the cavity. For four selected free-stream velocities, U_∞ = 341, 426, 514, and 585 ft/s,

pressure fluctuations inside the cavity were measured at $\theta = \pm 2°, \pm 4°, \pm 6°,$ and $\pm 10°$. Selected cavitypressure flucutations also were measured for d = 0.225 in. and b = 0.475 in. Throughout the present experiments of the fuze-nose model, the leading edge of the cavity was fixed at X_0 = 2.1 in. from the leading edge of the fuze nose.

Experiments were performed also on the fuze-nose cavity model to determine the minimum depth, d_{min}, needed for onset of cavity-flow oscillations. The value of d_{min} was determined for three axial locations: X_0 = 0.75, 1.25, and 2.10 in. from the leading edge of the fuze nose.

2.2 Instrumentation and Measurements

Constant-temperature, hot-wire anemometry was used extensively to determine the mean and the fluctuating velocity components of cavity-flow oscillations. Two hot-wire probes were employed which could be moved individually along the x and across the y directions of the cavity shear layer. The experimental setup was constructed to provide circumferential motion of these two hot wires relative to each other. The dc outputs of the hot wires, which are proportional to the mean velocities, were recorded on an X-Y plotter. The ac output signals of the hot wires, which are proportional to the velocity fluctuations in the cavity shear layer, were analyzed on an all-digital, real-time spectrum analyzer. The outputs of the two hot wires were cross correlated on a correlation and probability analyzer, which is an all-digital high-speed processing instrument and provides real-time computation for auto correlations and cross correlations. The output of the correlation was either displayed on an oscilloscope or plotted on an X-Y plotter.

The pressure fluctuations of the flow inside the cavity were measured with

a 1/8-in. pressure transducer, which was flush-mounted on the base of the cavity. The rise time of this transducer was 2 μs. The frequency response of the pressure transducer was from 2 to 40,000 Hz. The output of the pressure transducer was amplified 100 times and then passed through a filter to remove the component of the signal caused by the vibration of the system. The root mean square (rms) value of the pressure signal was measured on a time-averaging rms voltmeter. The signal was also analyzed on a spectrum analyzer to determine frequency distribution. From this, the mean square pressure fluctuations at the frequency of cavity flow oscillations were estimated as a function of cavity flow for each cavity configuration.

2.3 Flow Visualization

Flow near the cavity was visualized by injecting a small amount of CO_2 gas through the base of the cavity. Still shadowgraphs were taken with a spark source that had a duration of approximately 1.0 μs. A two-mirror Schlieren System was used as shown in Figure 3 to take high-speed motion pictures up to 7000 frames/s. The spark source, which had a duration of 0.3 μs, was triggered by the camera. This time was short enough to "freeze" the motion of the cavity flow field.

3. EXPERIMENTAL RESULTS

3.1 Visualization of Cavity Flow

The shadowgraph pictures of Figure 4 indicate the influence of angle of attack, α, of the free stream with respect to the axis of the axisymmetric cavity for values of $b = 0.68$ in., $d = 0.75$ in., and $U_\infty = 60$ ft/s. At $\alpha = 0$, the organized large-scale structures in the cavity shear layer can be seen in this

shadowgraph to be circumferentially symmetrical. At $\alpha = 4°$, however, structures were destroyed in the vicinity of the circumferential location, $\phi = 180°$, i.e., at the lower side of the cavity. On the upper side of the cavity ($\phi = 0°$), the organized structures were not affected by the angle of attack. The circumferential distribution of the fluctuating velocity in the cavity shear layer indicated that at an angle of attack the coherency of these structures was gradually destroyed as the circumferential position changed from $\phi = 0°$ to $\phi = 180°$. Similar behavior was evident for other cavity configurations, as Figures 5 and 6 indicate for $\alpha = 4°$ and $6°$, respectively.

Several series of high-speed Schlieren motion picture frames showing the effects of angle of attack on the formation of large-scale organized structures at b = 0.68 in., d = 0.25 in., and U_∞ = 60 ft/s are shown in Figures 7, 8, and 9 at $\alpha = 0°$, 3.5° and -3.5°, respectively. The cavity was oscillating in the second mode with nondimensional frequency $fb/U_\infty = 1.69$, where f = 1785 Hz. At $\alpha = 0°$ (Figure 7), the rollup of an organized structure is evident from frame 1 onwards. As the rollup of this convecting large organized structure continued, it engulfed the cavity fluid (which was made visible when a small amount of CO_2 gas was injected) into the free-stream potential fluid. Some of the cavity fluid engulfed by the free-stream potential fluid. Some of the cavity fluid engulfed by the organized large-scale cavity structure can be inferred in Figure 7, frame 4. The cavity fluid, which is carried by the large organized cavity structure, remained unmixed with the free-stream fluid as far as three to four wavelengths downstream from the downstream edge of the cavity. The wavelength is here defined as that of the organized large eddies in the cavity shear layer, i.e., $\lambda = U_c/f$.

At $\alpha = 3.5°$, Figure 8 shows the cavity oscillations close to $\phi = 0°$. As

indicated in the instant spark shadowgraphs of Figures 4 to 6, the high-speed Schlieren motion picture frames shown in Figure 8 indicated that the cavity flow was not altered significantly by the angle of attack. Closer examination of these high-speed picture frames, however, revealed that the oscillations around $\phi = 0°$ were even more organized for $0° < \alpha \leq 6°$ as compared with $\alpha = 0°$. For $6° < \alpha \leq 10°$, these large-scale structures again became less organized. The pressure fluctuations inside the cavity were accordingly modified by the angle of attack (section 3.2). There seemed to be a very close relationship of the coherency of organized structures in the cavity shear layer and the pressure oscillations inside the cavity.

Around $\phi = 180°$, on the other hand, the organized large-scale structures were very sensitive to the angle of attack. As shown in Figure 9, these structures were almost destroyed at an angle of attack of -3.5°. These results are in accordance with the still shadowgraphs shown in Figures 4 to 6.

3.2 Cavity Pressure Fluctuations at Angle of Attack

The influence of angle of attack on pressure fluctuations inside the cavity was determined for d = 0.1 in. and for b = 0.3, 0.4, and 0.475 in. at U_∞ = 426, 514, and 585 ft/s. Tests were performed also at the above free-stream velocities as well as at U_∞ = 341 ft/s for b = 0.475 in. and d = 0.225 in. Pressure fluctuations inside the cavity were measured at locations $\phi = 0°$, 60°, and 90°. At these cavity flow conditions and configurations, tests were conducted at $\alpha = \pm 2°, \pm 4°, \pm 6°$ and $\pm 10°$. Because of the symmetry of the axisymmetric flow, the above combinations of the values of ϕ and α were sufficient to infer the pressure oscillations over the entire 360° around the cavity. In all, 64 sets of data were taken. The data are tabulated in Tables 1 to 16.

The present results showed that the frequency of cavity-flow oscillations was independent of the angle of attack for a given cavity configuration and free-stream velocity.

The present results in Tables 1 to 16 indicate that the rms pressure fluctuations inside the cavity are very sensitive to the angle of attack. Figure 10 shows typical results of filtered rms pressure fluctuation, $\tilde{p}_{FILTERED}$, normalized with the free-stream dynamic pressure, $(1/2)\ \rho_\infty U_\infty^2$, for b = 0.475 in ., d = 0.225 in., and U_∞ = 341 ft/s. Results for four circumferential locations ϕ = 0°, 30°, 60°, and 90° are plotted in Figure 10. At α = 0° for ϕ = 0°, the rms pressure fluctuations were about 1.4% of the free-stream dynamic pressure. As α was increased further, the strength of the pressure oscillations due to cavity flow oscillation decreased in magnitude. As one would expect, the magnitudes of the pressure fluctuations for ϕ = 0°, 30°, 60°, and 90° at α = 0° were almost identical because the flow oscillations were circumferentially axisymmetric. At an angle of attack for ϕ = 30°, 60°, and 90°, the cavity pressure fluctuation peaked around α = 2°. Relatively, the rms pressure fluctuations for ϕ = 0°, 30°, 60° and 90° for $-10° \leq \alpha < 0°$ were less sensitive to the angle of attack than for $0° \leq \alpha \leq 10°$.

Figure 11 indicated the influence of the angle of attack on the filtered pressure in terms of total cavity rms pressure fluctuations at b = 0.475 in., d = 0.225 in., and U_∞ = 341 ft/s. At ϕ = 0° and α = 0°, only about 43% of the cavity rms pressure fluctuations was at cavity oscillation frequency. At about α = 4°, most of the pressure fluctuations were at the cavity oscillation frequency. Due to a superimposed random signal on the cavity pressure fluctuations, $\tilde{p}_{FILTERED}/\tilde{p}_{TOTAL} < 1$ was observed at the other transducer locations. Also as indicated in Figure 11, due to disorganized cavity fluctuations at ϕ = 0°, 30°, 60°,

and 90° for $\alpha < 0°$, only a small fraction of the cavity rms pressure fluctuations was observed at the cavity oscillation frequency.

Figures 12 and 13 show cavity pressure oscillations as in Figures 10 and 11, but for U_∞ = 585 ft/s. Similar deductions as drawn above apply to these results. Tables 1 to 16 list cavity pressure fluctuations for other flow speeds and cavity configurations.

3.3 Growth of Cavity Shear Layer

Recently, the growth of free-shear flows has been closely linked to the presence of the large-scale organized structures in them (Ref. 7 and 8). The velocity fluctuations in the oscillating cavity shear flow are organized because of the strong feedback resulting from the shear flow interaction with the downstream cavity corner. Such organized cavity flows have been shown to grow very rapidly (Ref. 5 and 6).

This section presents the results pertaining to the influence of the angle of attack on the growth of the cavity shear layer at various spanwise locations. Mean velocities in the cavity flow were obtained experimentally to determine the growth rate of the cavity shear layer. Detailed measurements were made with a fixed upstream Reynolds number $Re_{\theta_0} = 1.38 \times 10^2$, fixed width $b/\theta_0 = 185$, and fixed depth $d/\theta_0 = 50$. From these mean velocity profiles, the momentum thickness, θ, was determined:

$$\theta = \int_{-\infty}^{\infty} \frac{U}{U_\infty} \left(1 - \frac{U}{U_\infty}\right) dy ,$$

Inside the cavity, the integration was terminated where U(y) was approximately 5% to 7% of the mean free-stream velocity. In this region, the accuracy of the hot-wire measurements is doubtful. The growths of the cavity shear

layer for $\alpha = 0°$ and $3°$ at $\phi = 0°$ are indicated in Figure 14. Also shown are the growth rates, $d\theta/dx$, which represent the entrainment rates of the shear layer. The increased entrainment rate for $\alpha = 3°$ seems to result from locally enhanced periodic velocity fluctuations in the cavity shear layer. This increase, in turn, also results in increased pressure fluctuations inside the cavity as shown in Figures 10 to 13.

3.4 Minimum Depth for Oscillations at Different Cavity Locations

The minimum cavity depth for onset of cavity oscillations was determined at three axial locations: $X_0 = 0.75$, 1.25, and 2.10 in. from the leading edge of the fuze-nose cavity model. The depth was increased in steps of 0.010 in. for a fixed width. The free-stream velocity was varied from 0 to 700 ft/s. If no cavity flow oscillations were observed at velocities up to 700 ft/s, the depth was increased further up to 0.060 in.

For cavity location 0.75, no cavity oscillations were observed up to $U_\infty = 700$ ft/s and depths up to 0.60 in. for two widths, 0.2 and 0.3 in. However, a cavity located at 1.25 with $b = 0.25$ in. began to oscillate at $d_{min} = 0.050$ in. and at $U_\infty \approx 500$ ft/s. Then for a cavity location at 2.10 in. for width 0.325 in., no oscillations up to $U_\infty = 700$ ft/s were observed for $d = 0.020$, 0.030, and 0.040 in. At this location of 2.10 in., oscillations did not occur until $d_{min} = 0.050$ in. and $U_\infty \approx 420$ ft/s.

From the results it was concluded that, for the fuze-nose model, the upstream edge of the axisymmetric cavity should be located at $X_0 \geq 1.25$ in. The cavity flow will oscillate around $U_\infty \gtrsim 500$ ft/s with $b > 0.25$ in. and $d \geq 0.050$ in.

4. DISCUSSION AND CONCLUSIONS

A sketch of a fuse nose at an angle of attack is shown in Figure 15. On the upper side ($\phi \simeq 0°$), the free-stream flow along the model accelerates; consequently, the flow over the cavity in this vicinity is in a region of favorable pressure gradient. Cavity flow oscillations have been reported to be very pronounced when the cavity is located in the favorable (negative) pressure gradient (Ref. 5). This might have been one of the reasons for strong pressure fluctuations inside the cavity at $\phi \simeq 0°$ and at $\alpha = 2°$ to 6° as observed in Figures 10 to 14. In contrast, however, it can be inferred that the flow around the lower side ($\phi \simeq 180°$) is in an adverse pressure gradient region. Such flows over cavities tend to suppress cavity flow oscillations. Still shadowgraphs in Figures 4 to 6 and high-speed motion pictures in Figure 9 clearly indicate a disorganized flow over the cavity located in an adverse pressure gradient. This disorganization explains the loss of periodic pressure fluctuations inside the cavity as indicated in Figures 10 to 14 for $\alpha < 0°$ at $\phi = 0°$, 30°, 60°, and 90°.

The experimental results of flow visualization pictures indicate a close relationship of organized cavity flow oscillations to the pressure fluctuations inside the cavity. Due to the variation of circumferential coherency of these large-scale structures at an angle of attack, there were associated circumferential variations in the periodic cavity pressure fluctuations (Figures 10 to 13 and Tables 1 to 16). These data illustrate that the production of cavity pressure fluctuations results from the interaction of these organized large-scale structures with the downstream corner of the cavity. Also, pressure fluctuations inside the cavity are generated "locally" by the interaction of the cavity shear flow

with the downstream corner.

From the results of pressure measurements presented in Tables 1 to 16, for an oscillating cavity flow at an angle of attack, strong oscillations are always present in certain circumferential regions of the axisymmetric cavity.

The enhanced growth of the cavity shear layer at an angle of attack as indicated in Figure 14 indicates that the organized large-scale structures are important in its growth. These organized eddies engulf the cavity fluid and carry it into the potential flow surrounding the cavity. This engulfed fluid remains unmixed for many wavelengths of the convecting large-scale structures downstream from the cavity.

Because of the differential pressure imposed on the axisymmetric cavity flow at an angle of attack, there is circumferential fluid motion inside the cavity. This fluid motion can influence cavity flow oscillations and may have been the cause of loss of the magnitude of the cavity pressure fluctuations at large angles of attack, i.e., as shown in Tables 1 to 16. The role of this cross flow both around the axisymmetric body and inside the cavity need further attention.

NOMENCLATURE

b	Cavity width (Figure 1)
d	Cavity depth (Figure 1)
D	Outside diameter of axisymmetric body (Figure 1)
f	Frequency in hertz
$\tilde{p} \equiv \sqrt{\overline{p'^2}}$	Root mean square pressure fluctuations
R	Outside radius of axisymmetric body (Figure 1)
Re_D	Reynolds number based on diameter (Figure 1)
Re_{θ_0}	Reynolds number based on momentum thickness
S	Distance along the axisymmetric body (Figure 1)
$U(y)$	Mean velocity in x direction
U_c	Propagation speed of disturbances in the cavity shear layer
U_∞	Free-stream velocity
x	Streamwise coordinate from upstream cavity corner
X	Streamwise distance (Figure 1)
X_0	Location of upstream cavity corner (Figure 1)
y	Transverse coordinate

α	Angle of attack between free-stream flow and cavity axis (see insert in Figure 10)
ϕ	Circumferential location of transducer (see insert in Figure 10)
λ	Wavelength of propagating disturbance in shear layer
ρ_∞	Density of ambient air
θ	Shear layer momentum thickness
θ_o	Shear layer momentum thickness at separation where x = 0
$\frac{fb}{U_\infty}$	Nondimensional frequency

Subscripts

$( )_{min}$	Conditions for onset of cavity oscillations
$( )_{FILTERED}$	Filtered signal at cavity oscillation frequency
$( )_{TOTAL}$	Total output signal

REFERENCES

1. L. F. East, "Aerodynamic Induced Resonance in Rectangular Cavities," J. Sound and Vibrations, Vol. 3, March 1966, pp. 277-287.

2. K. Karamcheti, "Sound Radiated from Surface Cutouts in High-Speed Flows," Ph.D. Thesis, California Institute of Technology, June 1956.

3. A. Roshko," Some Measurements of Flow in a Rectangular Cutout," National Aeronautics and Space Administration TN-3488, 1955.

4. V. Sarohia, "Experimental Investigation of Oscillations in Flows over Shallow Cavities," AIAA Journal, Vol. 15, July 1977, pp. 984-991.

5. V. Sarohia and P. F. Massier, "Investigation of Pressure Oscillations in Axisymmetric Cavity Flows," HDL-CR-025-1, September 1977.

6. V. Sarohia, "Experimental and Analytical Investigation of Oscillations in Flows over Cavities," Ph.D. Thesis, Dept. of Aeronautics, California Institute of Technology, Pasadena, CA, March 1975.

7. R. L. Brown and A. Roshko, "On Density Effects and Large Scale Structures in Turbulent Mixing Layer," J. Fluid Mechanics, Vol. 64, Part 4, 1974, pp. 775-816.

8. C. D. Winant and D. F. Browand, "Vortex Paring: The Mechanism of Turbulent Mixing-Layer Growth at Moderate Reynolds Number," J. Fluid Mechanics, Vol. 63, 1974, pp. 237-255.

9. W. W. Willmarth, et al., "Management of Turbulent Shear Layers in Separated Flows," J. Aircraft, Vol. 15, July 1978, pp. 385-386.

TABLE 1

EFFECT OF ANGLE OF ATTACK ON PRESSURE OSCILLATIONS INSIDE CAVITY

WIDTH, b = 0.3 in.

DEPTH, d = 0.1 in.

LOCATION, ϕ = 0°

Angle of Attack, $\alpha°$	U_∞ = 341 ft/s				U_∞ = 426 ft/s				U_∞ = 514 ft/s				U_∞ = 585 ft/s			
	$\tilde{p}_{FILTERED}$ psi	$\frac{\tilde{p}_{FILTERED}}{\frac{1}{2}\rho_\infty U_\infty^2}$	$\tilde{p}_{TOTAL}$ psi	$\frac{\tilde{p}_{FILTERED}}{\tilde{p}_{TOTAL}}$	$\tilde{p}_{FILTERED}$ psi	$\frac{\tilde{p}_{FILTERED}}{\frac{1}{2}\rho_\infty U_\infty^2}$	$\tilde{p}_{TOTAL}$ psi	$\frac{\tilde{p}_{FILTERED}}{\tilde{p}_{TOTAL}}$	$\tilde{p}_{FILTERED}$ psi	$\frac{\tilde{p}_{FILTERED}}{\frac{1}{2}\rho_\infty U_\infty^2}$	$\tilde{p}_{TOTAL}$ psi	$\frac{\tilde{p}_{FILTERED}}{\tilde{p}_{TOTAL}}$	$\tilde{p}_{FILTERED}$ psi	$\frac{\tilde{p}_{FILTERED}}{\frac{1}{2}\rho_\infty U_\infty^2}$	$\tilde{p}_{TOTAL}$ psi	$\frac{\tilde{p}_{FILTERED}}{\tilde{p}_{TOTAL}}$
0					0.020	0.014	0.050	0.404	0.053	0.025	0.102	0.526	0.095	0.035	0.147	0.649
2					0.015	0.010	0.044	0.340	0.048	0.022	0.087	0.547	0.067	0.024	0.131	0.514
4					0.011	0.007	0.041	0.263	0.030	0.014	0.076	0.396	0.040	0.015	0.118	0.341
6					0.008	0.005	0.039	0.196	0.023	0.010	0.071	0.317	0.038	0.014	0.114	0.332
10									0.015	0.007	0.066	0.229	0.036	0.013	0.107	0.334
-2					0.015	0.010	0.057	0.266	0.064	0.029	0.106	0.597	0.090	0.033	0.158	0.567
-4					0.013	0.009	0.066	0.204	0.042	0.020	0.110	0.387	0.067	0.024	0.160	0.420
-6					0.008	0.006	0.078	0.109	0.023	0.010	0.122	0.184	0.034	0.012	0.170	0.198
-10									0.013	0.006	0.187	0.068	0.019	0.007	0.230	0.083

TABLE 2
EFFECT OF ANGLE OF ATTACK ON PRESSURE
OSCILLATIONS INSIDE CAVITY

WIDTH, b = 0.3 in.

DEPTH, d = 0.1 in.

LOCATION, ϕ = 30°

Angle of attack, α°	U_∞ = 341 ft/s				U_∞ = 426 ft/s				U_∞ = 514 ft/s				U_∞ = 585 ft/s			
	$\tilde{p}_{FILTERED}$ psi	$\frac{\tilde{p}_{FILTERED}}{\frac{1}{2}\rho_\infty U_\infty^2}$	$\tilde{p}_{TOTAL}$ psi	$\frac{\tilde{p}_{FILTERED}}{\tilde{p}_{TOTAL}}$	$\tilde{p}_{FILTERED}$ psi	$\frac{\tilde{p}_{FILTERED}}{\frac{1}{2}\rho_\infty U_\infty^2}$	$\tilde{p}_{TOTAL}$ psi	$\frac{\tilde{p}_{FILTERED}}{\tilde{p}_{TOTAL}}$	$\tilde{p}_{FILTERED}$ psi	$\frac{\tilde{p}_{FILTERED}}{\frac{1}{2}\rho_\infty U_\infty^2}$	$\tilde{p}_{TOTAL}$ psi	$\frac{\tilde{p}_{FILTERED}}{\tilde{p}_{TOTAL}}$	$\tilde{p}_{FILTERED}$ psi	$\frac{\tilde{p}_{FILTERED}}{\frac{1}{2}\rho_\infty U_\infty^2}$	$\tilde{p}_{TOTAL}$ psi	$\frac{\tilde{p}_{FILTERED}}{\tilde{p}_{TOTAL}}$
0					0.021	0.015	0.052	0.410	0.060	0.028	0.100	0.600	0.095	0.035	0.150	0.635
2					0.015	0.010	0.045	0.332	0.045	0.021	0.089	0.507	0.064	0.023	0.133	0.479
4					0.009	0.006	0.043	0.210	0.028	0.013	0.079	0.359	0.048	0.017	0.123	0.388
6					0.008	0.005	0.037	0.202	0.036	0.017	0.077	0.464	0.048	0.017	0.122	0.391
10									0.023	0.010	0.064	0.351	0.042	0.015	0.108	0.393
-2					0.014	0.010	0.055	0.258	0.060	0.028	0.107	0.561	0.095	0.035	0.166	0.574
-4					0.010	0.007	0.065	0.154	0.042	0.020	0.111	0.382	0.067	0.024	0.165	0.409
-6					0.009	0.006	0.079	0.113	0.021	0.010	0.125	0.171	0.038	0.014	0.176	0.215
-10									0.012	0.006	0.17[illegible]	0.068	0.019	0.007	0.225	0.084

TABLE 3

EFFECT OF ANGLE OF ATTACK ON PRESSURE OSCILLATIONS INSIDE CAVITY

WIDTH, b = 0.3 in.

DEPTH, d = 0.1 in.

LOCATION, ϕ = 60°

Angle of attack, α°	U_∞ = 341 ft/s				U_∞ = 426 ft/s				U_∞ = 514 ft/s				U_∞ = 585 ft/s			
	$\tilde{p}_{FILTERED}$ psi	$\frac{\tilde{p}_{FILTERED}}{\frac{1}{2}\rho_\infty U_\infty^2}$	$\tilde{p}_{TOTAL}$ psi	$\frac{\tilde{p}_{FILTERED}}{\tilde{p}_{TOTAL}}$	$\tilde{p}_{FILTERED}$ psi	$\frac{\tilde{p}_{FILTERED}}{\frac{1}{2}\rho_\infty U_\infty^2}$	$\tilde{p}_{TOTAL}$ psi	$\frac{\tilde{p}_{FILTERED}}{\tilde{p}_{TOTAL}}$	$\tilde{p}_{FILTERED}$ psi	$\frac{\tilde{p}_{FILTERED}}{\frac{1}{2}\rho_\infty U_\infty^2}$	$\tilde{p}_{TOTAL}$ psi	$\frac{\tilde{p}_{FILTERED}}{\tilde{p}_{TOTAL}}$	$\tilde{p}_{FILTERED}$ psi	$\frac{\tilde{p}_{FILTERED}}{\frac{1}{2}\rho_\infty U_\infty^2}$	$\tilde{p}_{TOTAL}$ psi	$\frac{\tilde{p}_{FILTERED}}{\tilde{p}_{TOTAL}}$
0					0.016	0.011	0.047	0.343	0.060	0.028	0.091	0.656	0.085	0.031	0.134	0.634
2					0.012	0.008	0.042	0.283	0.042	0.020	0.082	0.516	0.067	0.024	0.123	0.547
4					0.012	0.008	0.039	0.307	0.032	0.015	0.078	0.411	0.053	0.019	0.117	0.457
6					0.010	0.007	0.039	0.247	0.030	0.014	0.072	0.417	0.042	0.015	0.110	0.387
10									0.020	0.009	0.059	0.342	0.030	0.011	0.090	0.335
-2					0.017	0.012	0.052	0.326	0.053	0.025	0.095	0.565	0.085	0.031	0.139	0.612
-4					0.010	0.007	0.060	0.159	0.036	0.017	0.096	0.371	0.060	0.022	0.136	0.440
-6					0.008	0.006	0.073	0.117	0.029	0.009	0.105	0.181	0.032	0.012	0.139	0.229
-10									0.015	0.007	0.166	0.091	0.023	0.008	0.193	0.117

TABLE 4
EFFECT OF ANGLE OF ATTACK ON PRESSURE
OSCILLATIONS INSIDE CAVITY

WIDTH, b = 0.3 in.

DEPTH, d = 0.1 in.

LOCATION, ϕ = 90°

Angle of attack, α°	U_∞ = 341 ft/s				U_∞ = 426 ft/s				U_∞ = 514 ft/s				U_∞ = 585 ft/s			
	$\tilde{p}_{FILTERED}$ psi	$\frac{\tilde{p}_{FILTERED}}{\frac{1}{2}\rho_\infty U_\infty^2}$	$\tilde{p}_{TOTAL}$ psi	$\frac{\tilde{p}_{FILTERED}}{\tilde{p}_{TOTAL}}$	$\tilde{p}_{FILTERED}$ psi	$\frac{\tilde{p}_{FILTERED}}{\frac{1}{2}\rho_\infty U_\infty^2}$	$\tilde{p}_{TOTAL}$ psi	$\frac{\tilde{p}_{FILTERED}}{\tilde{p}_{TOTAL}}$	$\tilde{p}_{FILTERED}$ psi	$\frac{\tilde{p}_{FILTERED}}{\frac{1}{2}\rho_\infty U_\infty^2}$	$\tilde{p}_{TOTAL}$ psi	$\frac{\tilde{p}_{FILTERED}}{\tilde{p}_{TOTAL}}$	$\tilde{p}_{FILTERED}$ psi	$\frac{\tilde{p}_{FILTERED}}{\frac{1}{2}\rho_\infty U_\infty^2}$	$\tilde{p}_{TOTAL}$ psi	$\frac{\tilde{p}_{FILTERED}}{\tilde{p}_{TOTAL}}$
0					0.023	0.015	0.041	0.548	0.053	0.025	0.083	0.645	0.085	0.031	0.130	0.652
2					0.016	0.011	0.041	0.393	0.048	0.022	0.081	0.586	0.071	0.026	0.123	0.580
4					0.013	0.009	0.040	0.316	0.038	0.018	0.076	0.499	0.053	0.019	0.117	0.459
6					0.008	0.005	0.042	0.179	0.028	0.013	0.071	0.402	0.042	0.015	0.108	0.393
10									0.013	0.006	0.081	0.165	0.018	0.007	0.115	0.156
-2					0.015	0.010	0.042	0.357	0.053	0.025	0.083	0.645	0.071	0.026	0.124	0.577
-4					0.011	0.008	0.043	0.261	0.040	0.019	0.077	0.521	0.060	0.022	0.115	0.522
-6					0.008	0.005	0.047	0.172	0.024	0.011	0.074	0.324	0.034	0.012	0.107	0.314
-10									0.013	0.006	0.091	0.139	0.020	0.007	0.123	0.163

TABLE 5
EFFECT OF ANGLE OF ATTACK ON PRESSURE
OSCILLATIONS INSIDE CAVITY

WIDTH, b = 0.4 in.

DEPTH, d = 0.1 in.

LOCATION, ϕ = 0°

Angle of attack, α°	U_∞ = 341 ft/s				U_∞ = 426 ft/s				U_∞ = 514 ft/s				U_∞ = 585 ft/s			
	$\tilde{p}_{FILTERED}$ psi	$\tilde{p}_{FILTERED} / \frac{1}{2}\rho_\infty U_\infty^2$	$\tilde{p}_{TOTAL}$ psi	$\tilde{p}_{FILTERED} / \tilde{p}_{TOTAL}$	$\tilde{p}_{FILTERED}$ psi	$\tilde{p}_{FILTERED} / \frac{1}{2}\rho_\infty U_\infty^2$	$\tilde{p}_{TOTAL}$ psi	$\tilde{p}_{FILTERED} / \tilde{p}_{TOTAL}$	$\tilde{p}_{FILTERED}$ psi	$\tilde{p}_{FILTERED} / \frac{1}{2}\rho_\infty U_\infty^2$	$\tilde{p}_{TOTAL}$ psi	$\tilde{p}_{FILTERED} / \tilde{p}_{TOTAL}$	$\tilde{p}_{FILTERED}$ psi	$\tilde{p}_{FILTERED} / \frac{1}{2}\rho_\infty U_\infty^2$	$\tilde{p}_{TOTAL}$ psi	$\tilde{p}_{FILTERED} / \tilde{p}_{TOTAL}$
0					0.027	0.018	0.040	0.668	0.107	0.049	0.121	0.879	0.169	0.061	0.190	0.891
2					0.030	0.021	0.039	0.781	0.095	0.044	0.113	.839	0.142	0.052	0.168	0.845
4					0.020	0.014	0.032	0.626	0.080	0.037	0.097	0.822	0.107	0.039	0.146	0.731
6					0.014	0.010	0.027	0.522	0.060	0.028	0.082	0.733	0.113	0.041	0.134	0.843
10					0.010	0.007	0.025	0.409	0.030	0.014	0.060	0.502	0.067	0.024	0.105	0.639
-2					0.025	0.017	0.044	0.570	0.107	0.049	0.126	0.849	0.169	0.061	0.201	0.843
-4					0.017	0.012	0.051	0.329	0.090	0.042	0.115	0.781	0.160	0.058	0.197	0.811
-6					0.013	0.009	0.063	0.213	0.045	0.021	0.106	0.423	0.127	0.046	0.170	0.748
-10					0.013	0.009	0.093	0.137	0.020	0.009	0.135	0.143	0.032	0.012	0.174	0.183

TABLE 6
EFFECT OF ANGLE OF ATTACK ON PRESSURE OSCILLATIONS INSIDE CAVITY

WIDTH, b = 0.4 in.

DEPTH, d = 0.1 in.

LOCATION, ϕ = 30°

Angle of attack, α°	U_∞ = 341 ft/s				U_∞ = 426 ft/s				U_∞ = 514 ft/s				U_∞ = 585 ft/s			
	$\tilde{p}_{FILTERED}$ psi	$\tilde{p}_{FILTERED}/\frac{1}{2}\rho_\infty U_\infty^2$	$\tilde{p}_{TOTAL}$ psi	$\tilde{p}_{FILTERED}/\tilde{p}_{TOTAL}$	$\tilde{p}_{FILTERED}$ psi	$\tilde{p}_{FILTERED}/\frac{1}{2}\rho_\infty U_\infty^2$	$\tilde{p}_{TOTAL}$ psi	$\tilde{p}_{FILTERED}/\tilde{p}_{TOTAL}$	$\tilde{p}_{FILTERED}$ psi	$\tilde{p}_{FILTERED}/\frac{1}{2}\rho_\infty U_\infty^2$	$\tilde{p}_{TOTAL}$ psi	$\tilde{p}_{FILTERED}/\tilde{p}_{TOTAL}$	$\tilde{p}_{FILTERED}$ psi	$\tilde{p}_{FILTERED}/\frac{1}{2}\rho_\infty U_\infty^2$	$\tilde{p}_{TOTAL}$ psi	$\tilde{p}_{FILTERED}/\tilde{p}_{TOTAL}$
0					0.030	0.021	0.041	0.740	0.120	0.055	0.127	0.945	0.160	0.058	0.173	0.921
2					0.024	0.016	0.037	0.647	0.095	0.044	0.109	0.876	0.151	0.055	0.172	0.875
4					0.019	0.013	0.032	0.601	0.090	0.042	0.101	0.893	0.134	0.049	0.160	0.837
6					0.015	0.010	0.027	0.553	0.076	0.035	0.090	0.836	0.120	0.044	0.142	0.845
10					0.008	0.005	0.023	0.328	0.034	0.016	0.057	0.590	0.071	0.026	0.107	0.667
-2					0.024	0.016	0.044	0.545	0.127	0.059	0.134	0.949	0.179	0.065	0.190	0.944
-4					0.015	0.010	0.051	0.297	0.107	0.049	0.116	0.919	0.160	0.058	0.181	0.883
-6					0.011	0.008	0.062	0.182	0.053	0.025	0.103	0.521	0.101	0.037	0.160	0.628
-10					0.011	0.007	0.096	0.111	0.023	0.010	0.143	0.157	0.030	0.011	0.180	0.167

TABLE 7
EFFECT OF ANGLE OF ATTACK ON PRESSURE OSCILLATIONS INSIDE CAVITY

WIDTH, b = 0.4 in.

DEPTH, d = 0.1 in.

LOCATION, ϕ = 60°

Angle of attack, α°	U_∞ = 341 ft/s				U_∞ = 426 ft/s				U_∞ = 514 ft/s				U_∞ = 585 ft/s			
	$\tilde{p}_{FILTERED}$ psi	$\tilde{p}_{FILTERED}/\frac{1}{2}\rho_\infty U_\infty^2$	$\tilde{p}_{TOTAL}$ psi	$\tilde{p}_{FILTERED}/\tilde{p}_{TOTAL}$	$\tilde{p}_{FILTERED}$ psi	$\tilde{p}_{FILTERED}/\frac{1}{2}\rho_\infty U_\infty^2$	$\tilde{p}_{TOTAL}$ psi	$\tilde{p}_{FILTERED}/\tilde{p}_{TOTAL}$	$\tilde{p}_{FILTERED}$ psi	$\tilde{p}_{FILTERED}/\frac{1}{2}\rho_\infty U_\infty^2$	$\tilde{p}_{TOTAL}$ psi	$\tilde{p}_{FILTERED}/\tilde{p}_{TOTAL}$	$\tilde{p}_{FILTERED}$ psi	$\tilde{p}_{FILTERED}/\frac{1}{2}\rho_\infty U_\infty^2$	$\tilde{p}_{TOTAL}$ psi	$\tilde{p}_{FILTERED}/\tilde{p}_{TOTAL}$
0					0.030	0.021	0.040	0.760	0.127	0.059	0.127	1.000	0.169	0.061	0.171	0.988
2					0.025	0.017	0.037	0.686	0.095	0.044	0.109	0.876	0.160	0.058	0.170	0.939
4					0.018	0.012	0.033	0.540	0.095	0.044	0.108	0.880	0.151	0.055	0.167	0.900
6					0.013	0.009	0.030	0.449	0.076	0.035	0.093	0.816	0.120	0.044	0.143	0.835
10					0.010	0.007	0.030	0.318	0.030	0.014	0.061	0.493	0.057	0.021	0.104	0.543
-2					0.025	0.017	0.042	0.599	0.120	0.055	0.124	0.965	0.151	0.055	0.174	0.867
-4					0.019	0.013	0.047	0.403	0.090	0.042	0.107	0.839	0.142	0.052	0.164	0.870
-6					0.015	0.010	0.058	0.259	0.064	0.029	0.096	0.660	0.095	0.035	0.151	0.631
-10					0.013	0.009	0.087	0.154	0.021	0.010	0.130	0.163	0.036	0.013	0.166	0 216

TABLE 8
EFFECT OF ANGLE OF ATTACK ON PRESSURE
OSCILLATIONS INSIDE CAVITY

WIDTH, b = 0.4 in.

DEPTH, d = 0.1 in.

LOCATION, ϕ = 90°

Angle of attack, α°	U_∞ = 341 ft/s				U_∞ = 426 ft/s				U_∞ = 514 ft/s				U_∞ = 585 ft/s			
	$\tilde{p}_{FILTERED}$ psi	$\tilde{p}_{FILTERED} / \frac{1}{2}\rho_\infty U_\infty^2$	$\tilde{p}_{TOTAL}$ psi	$\tilde{p}_{FILTERED} / \tilde{p}_{TOTAL}$	$\tilde{p}_{FILTERED}$ psi	$\tilde{p}_{FILTERED} / \frac{1}{2}\rho_\infty U_\infty^2$	$\tilde{p}_{TOTAL}$ psi	$\tilde{p}_{FILTERED} / \tilde{p}_{TOTAL}$	$\tilde{p}_{FILTERED}$ psi	$\tilde{p}_{FILTERED} / \frac{1}{2}\rho_\infty U_\infty^2$	$\tilde{p}_{TOTAL}$ psi	$\tilde{p}_{FILTERED} / \tilde{p}_{TOTAL}$	$\tilde{p}_{FILTERED}$ psi	$\tilde{p}_{FILTERED} / \frac{1}{2}\rho_\infty U_\infty^2$	$\tilde{p}_{TOTAL}$ psi	$\tilde{p}_{FILTERED} / \tilde{p}_{TOTAL}$
0					0.030	0.021	0.039	0.770	0.095	0.044	0.112	0.851	0.169	0.061	0.178	0.952
2					0.027	0.018	0.036	0.737	0.095	0.044	0.111	0.859	0.169	0.061	0.183	0.922
4					0.020	0.014	0.035	0.569	0.095	0.044	0.111	0.855	0.160	0.058	0.178	0.899
6					0.012	0.008	0.037	0.320	0.080	0.037	0.090	0.891	0.127	0.046	0.146	0.869
10					0.008	0.006	0.050	0.170	0.023	0.010	0.079	0.287	0.050	0.018	0.119	0.425
-2					0.028	0.019	0.039	0.727	0.107	0.049	0.115	0.928	0.160	0.058	0.171	0.936
-4					0.017	0.012	0.040	0.427	0.085	0.039	0.101	0.843	0.120	0.044	0.151	0.791
-6					0.011	0.008	0.045	0.252	0.053	0.025	0.087	0.613	0.107	0.039	0.146	0.731
-10					0.009	0.006	0.060	0.149	0.024	0.011	0.094	0.255	0.040	0.015	0.132	0.304

TABLE 9
EFFECT OF ANGLE OF ATTACK ON PRESSURE
OSCILLATIONS INSIDE CAVITY

WIDTH, b = 0.475 in.

DEPTH, d = 0.1 in.

LOCATION, ϕ = 0°

Angle of attack, α°	U_∞ = 341 ft/s				U_∞ = 426 ft/s				U_∞ = 514 ft/s				U_∞ = 585 ft/s			
	$\tilde{p}_{FILTERED}$ psi	$\frac{\tilde{p}_{FILTERED}}{\frac{1}{2}\rho_\infty U_\infty^2}$	$\tilde{p}_{TOTAL}$ psi	$\frac{\tilde{p}_{FILTERED}}{\tilde{p}_{TOTAL}}$	$\tilde{p}_{FILTERED}$ psi	$\frac{\tilde{p}_{FILTERED}}{\frac{1}{2}\rho_\infty U_\infty^2}$	$\tilde{p}_{TOTAL}$ psi	$\frac{\tilde{p}_{FILTERED}}{\tilde{p}_{TOTAL}}$	$\tilde{p}_{FILTERED}$ psi	$\frac{\tilde{p}_{FILTERED}}{\frac{1}{2}\rho_\infty U_\infty^2}$	$\tilde{p}_{TOTAL}$ psi	$\frac{\tilde{p}_{FILTERED}}{\tilde{p}_{TOTAL}}$	$\tilde{p}_{FILTERED}$ psi	$\frac{\tilde{p}_{FILTERED}}{\frac{1}{2}\rho_\infty U_\infty^2}$	$\tilde{p}_{TOTAL}$ psi	$\frac{\tilde{p}_{FILTERED}}{\tilde{p}_{TOTAL}}$
0					0.045	0.031	0.052	0.859	0.127	0.059	0.144	0.882	0.213	0.077	0.227	0.939
2					0.038	0.026	0.045	0.843	0.107	0.049	0.126	0.849	0.169	0.061	0.190	0.891
4					0.032	0.022	0.037	0.851	0.120	0.055	0.123	0.973	0.179	0.065	0.184	0.971
6					0.017	0.012	0.036	0.472	0.095	0.044	0.115	0.827	0.151	0.055	0.160	0.939
10					0.010	0.007	0.034	0.278	0.053	0.025	0.081	0.658	0.085	0.031	0.121	0.698
-2					0.045	0.031	0.057	0.794	0.120	0.055	0.147	0.814	0.179	0.065	0.218	0.821
-4					0.025	0.017	0.056	0.455	0.107	0.049	0.135	0.792	0.169	0.061	0.213	0.795
-6					0.016	0.011	0.065	0.247	0.064	0.029	0.115	0.553	0.134	0.049	0.187	0.718
-10					0.008	0.006	0.083	0.102	0.021	0.010	0.132	0.161	0.034	0.012	0.158	0.213

TABLE 10
EFFECT OF ANGLE OF ATTACK ON PRESSURE
OSCILLATIONS INSIDE CAVITY

WIDTH, b = 0.475 in.

DEPTH, d = 0.1 in.

LOCATION, ϕ = 30°

Angle of attack, α°	U_∞ = 341 ft/s				U_∞ = 426 ft/s				U_∞ = 514 ft/s				U_∞ = 585 ft/s			
	$\tilde{p}_{FILTERED}$ psi	$\frac{\tilde{p}_{FILTERED}}{\frac{1}{2}\rho_\infty U_\infty^2}$	$\tilde{p}_{TOTAL}$ psi	$\frac{\tilde{p}_{FILTERED}}{\tilde{p}_{TOTAL}}$	$\tilde{p}_{FILTERED}$ psi	$\frac{\tilde{p}_{FILTERED}}{\frac{1}{2}\rho_\infty U_\infty^2}$	$\tilde{p}_{TOTAL}$ psi	$\frac{\tilde{p}_{FILTERED}}{\tilde{p}_{TOTAL}}$	$\tilde{p}_{FILTERED}$ psi	$\frac{\tilde{p}_{FILTERED}}{\frac{1}{2}\rho_\infty U_\infty^2}$	$\tilde{p}_{TOTAL}$ psi	$\frac{\tilde{p}_{FILTERED}}{\tilde{p}_{TOTAL}}$	$\tilde{p}_{FILTERED}$ psi	$\frac{\tilde{p}_{FILTERED}}{\frac{1}{2}\rho_\infty U_\infty^2}$	$\tilde{p}_{TOTAL}$ psi	$\frac{\tilde{p}_{FILTERED}}{\tilde{p}_{TOTAL}}$
0					0.040	0.027	0.064	0.630	0.127	0.059	0.141	0.902	0.213	0.077	0.223	0.955
2					0.032	0.022	0.058	0.552	0.142	0.066	0.142	1.000	0.213	0.077	0.213	1.000
4					0.019	0.013	0.056	0.341	0.134	0.062	0.134	1.000	0.179	0.065	0.184	0.971
6					0.013	0.009	0.053	0.237	0.085	0.039	0.107	0.792	0.142	0.052	0.152	0.934
10					0.008	0.005	0.052	0.144	0.028	0.013	0.058	0.492	0.071	0.026	0.107	0.667
-2					0.042	0.029	0.060	0.703	0.120	0.055	0.127	0.945	0.160	0.058	0.202	0.792
-4					0.027	0.018	0.064	0.421	0.085	0.039	0.116	0.730	0.151	0.055	0.195	0.772
-6					0.014	0.010	0.068	0.210	0.060	0.028	0.098	0.610	0.113	0.041	0.168	0.673
-10					0.008	0.006	0.088	0.097	0.021	0.010	0.121	0.176	0.042	0.015	0.153	0.278

TABLE 11
EFFECT OF ANGLE OF ATTACK ON PRESSURE
OSCILLATIONS INSIDE CAVITY

WIDTH, b = 0.475 in.

DEPTH, d = 0.1 in.

LOCATION, ϕ = 60°

Angle of attack, α°	U_∞ = 341 ft/s				U_∞ = 426 ft/s				U_∞ = 514 ft/s				U_∞ = 585 ft/s			
	$\tilde{p}_{FILTERED}$ psi	$\tilde{p}_{FILTERED} / \frac{1}{2}\rho_\infty U_\infty^2$	$\tilde{p}_{TOTAL}$ psi	$\tilde{p}_{FILTERED} / \tilde{p}_{TOTAL}$	$\tilde{p}_{FILTERED}$ psi	$\tilde{p}_{FILTERED} / \frac{1}{2}\rho_\infty U_\infty^2$	$\tilde{p}_{TOTAL}$ psi	$\tilde{p}_{FILTERED} / \tilde{p}_{TOTAL}$	$\tilde{p}_{FILTERED}$ psi	$\tilde{p}_{FILTERED} / \frac{1}{2}\rho_\infty U_\infty^2$	$\tilde{p}_{TOTAL}$ psi	$\tilde{p}_{FILTERED} / \tilde{p}_{TOTAL}$	$\tilde{p}_{FILTERED}$ psi	$\tilde{p}_{FILTERED} / \frac{1}{2}\rho_\infty U_\infty^2$	$\tilde{p}_{TOTAL}$ psi	$\tilde{p}_{FILTERED} / \tilde{p}_{TOTAL}$
0					0.036	0.024	0.061	0.586	0.127	0.059	0.140	0.909	0.213	0.077	0.216	0.988
2					0.034	0.023	0.056	0.601	0.134	0.062	0.138	0.974	0.213	0.077	0.216	0.988
4					0.024	0.016	0.050	0.475	0.107	0.049	0.115	0.928	0.151	0.055	0.176	0.854
6					0.021	0.015	0.052	0.406	0.095	0.044	0.096	0.993	0.113	0.041	0.144	0.783
10					0.010	0.007	0.053	0.178	0.036	0.017	0.075	0.477	0.060	0.022	0.116	0.517
-2					0.038	0.026	0.063	0.600	0.107	0.049	0.134	0.790	0.169	0.061	0.201	0.843
-4					0.023	0.015	0.062	0.364	0.085	0.039	0.120	0.704	0.169	0.061	0.189	.896
-6					0.013	0.009	0.065	0.194	0.067	0.031	0.104	0.646	0.101	0.037	0.168	0.598
-10					0.013	0.009	0.084	0.150	0.023	0.010	0.112	0.201	0.042	0.015	0.153	0.277

TABLE 12
EFFECT ON ANGLE OF ATTACK ON PRESSURE
OSCILLATIONS INSIDE CAVITY

WIDTH, b = 0.475 in.

DEPTH, d = 0.1 in.

LOCATION, ϕ = 90°

Angle of attack, α°	U_∞ = 341 ft/s				U_∞ = 426 ft/s				U_∞ = 514 ft/s				U_∞ = 585 ft/s			
	$\tilde{p}_{FILTERED}$ psi	$\frac{\tilde{p}_{FILTERED}}{\frac{1}{2}\rho_\infty U_\infty^2}$	$\tilde{p}_{TOTAL}$ psi	$\frac{\tilde{p}_{FILTERED}}{\tilde{p}_{TOTAL}}$	$\tilde{p}_{FILTERED}$ psi	$\frac{\tilde{p}_{FILTERED}}{\frac{1}{2}\rho_\infty U_\infty^2}$	$\tilde{p}_{TOTAL}$ psi	$\frac{\tilde{p}_{FILTERED}}{\tilde{p}_{TOTAL}}$	$\tilde{p}_{FILTERED}$ psi	$\frac{\tilde{p}_{FILTERED}}{\frac{1}{2}\rho_\infty U_\infty^2}$	$\tilde{p}_{TOTAL}$ psi	$\frac{\tilde{p}_{FILTERED}}{\tilde{p}_{TOTAL}}$	$\tilde{p}_{FILTERED}$ psi	$\frac{\tilde{p}_{FILTERED}}{\frac{1}{2}\rho_\infty U_\infty^2}$	$\tilde{p}_{TOTAL}$ psi	$\frac{\tilde{p}_{FILTERED}}{\tilde{p}_{TOTAL}}$
0					0.038	0.026	0.047	0.804	0.127	0.059	0.130	0.972	0.179	0.065	0.205	0.875
2					0.034	0.023	0.042	0.799	0.142	0.066	0.141	1.012	0.213	0.077	0.227	0.937
4					0.025	0.017	0.041	0.623	0.095	0.044	0.112	0.847	0.151	0.055	0.193	0.783
6					0.020	0.014	0.042	0.482	0.060	0.028	0.091	0.660	0.120	0.044	0.159	0.751
10					0.013	0.009	0.048	0.263	0.028	0.013	0.082	0.347	0.060	0.022	0.130	0.462
-2					0.028	0.019	0.045	0.625	0.101	0.047	0.118	0.856	0.160	0.058	0.189	0.846
-4					0.021	0.015	0.042	0.504	0.067	0.031	0.105	0.642	0.120	0.044	0.168	0.713
-6					0.016	0.011	0.042	0.378	0.071	0.033	0.094	0.762	0.090	0.033	0.157	0.573
-10					0.013	0.009	0.054	0.235	0.030	0.014	0.083	0.360	0.050	0.018	0.132	0.384

TABLE 13
EFFECT OF ANGLE OF ATTACK ON PRESSURE
OSCILLATIONS INSIDE CAVITY

WIDTH, b = 0.475 in.

DEPTH, d = 0.225 in.

LOCATION, ϕ = 0°

Angle of attack, α°	U_∞ = 341 ft/s				U_∞ = 426 ft/s				U_∞ = 514 ft/s				U_∞ = 585 ft/s			
	$\tilde{p}_{FILTERED}$ psi	$\frac{\tilde{p}_{FILTERED}}{\frac{1}{2}\rho_\infty U_\infty^2}$	$\tilde{p}_{TOTAL}$ psi	$\frac{\tilde{p}_{FILTERED}}{\tilde{p}_{TOTAL}}$	$\tilde{p}_{FILTERED}$ psi	$\frac{\tilde{p}_{FILTERED}}{\frac{1}{2}\rho_\infty U_\infty^2}$	$\tilde{p}_{TOTAL}$ psi	$\frac{\tilde{p}_{FILTERED}}{\tilde{p}_{TOTAL}}$	$\tilde{p}_{FILTERED}$ psi	$\frac{\tilde{p}_{FILTERED}}{\frac{1}{2}\rho_\infty U_\infty^2}$	$\tilde{p}_{TOTAL}$ psi	$\frac{\tilde{p}_{FILTERED}}{\tilde{p}_{TOTAL}}$	$\tilde{p}_{FILTERED}$ psi	$\frac{\tilde{p}_{FILTERED}}{\frac{1}{2}\rho_\infty U_\infty^2}$	$\tilde{p}_{TOTAL}$ psi	$\frac{\tilde{p}_{FILTERED}}{\tilde{p}_{TOTAL}}$
0	0.127	0.014	0.032	0.426	0.053	0.037	0.071	0.752	0.053	0.037	0.112	0.476	0.071	0.026	0.144	0.494
2	0.030	0.032	0.041	0.73	0.076	0.052	0.087	0.867	0.08	0.055	0.115	0.696	0.120	0.044	0.155	0.772
4	0.036	0.038	0.039	0.916	0.067	0.046	0.072	0.933	0.076	0.052	0.104	0.724	0.141	0.051	0.143	0.981
6	0.025	0.027	0.033	0.763	0.036	0.024	0.057	0.625	0.045	0.031	0.091	0.492	0.107	0.039	0.127	0.838
10	0.010	0.010	0.027	0.356	0.048	0.033	0.057	0.833	0.048	0.033	0.091	0.524	0.090	0.033	0.137	0.656
-2	0.007	0.008	0.012	0.171	0.034	0.023	0.073	0.461	0.341	0.028	0.123	0.334	0.08	0.029	0.163	0.491
-4	0.006	0.006	0.049	0.122	0.025	0.017	0.082	0.307	0.029	0.020	0.130	0.224	0.048	0.017	0.174	0.274
-6	0.007	0.007	0.062	0.109	0.025	0.017	0.099	0.256	0.033	0.022	0.154	0.212	0.030	0.011	0.198	0.152
-10	0.010	0.010	0.102	0.094	0.011	0.008	0.142	0.080	0.027	0.018	0.206	0.130	0.030	0.011	0.262	0.115

TABLE 14
EFFECT OF ANGLE OF ATTACK ON PRESSURE
OSCILLATIONS INSIDE CAVITY

WIDTH, b = 0.475 in.

DEPTH, d = 0.225 in.

LOCATION, ϕ = 30°

Angle of attack, α°	U_∞ = 341 ft/s				U_∞ = 426 ft/s				U_∞ = 514 ft/s				U_∞ = 585 ft/s			
	$\tilde{p}_{FILTERED}$ psi	$\tilde{p}_{FILTERED} / \frac{1}{2}\rho_\infty U_\infty^2$	$\tilde{p}_{TOTAL}$ psi	$\tilde{p}_{FILTERED} / \tilde{p}_{TOTAL}$	$\tilde{p}_{FILTERED}$ psi	$\tilde{p}_{FILTERED} / \frac{1}{2}\rho_\infty U_\infty^2$	$\tilde{p}_{TOTAL}$ psi	$\tilde{p}_{FILTERED} / \tilde{p}_{TOTAL}$	$\tilde{p}_{FILTERED}$ psi	$\tilde{p}_{FILTERED} / \frac{1}{2}\rho_\infty U_\infty^2$	$\tilde{p}_{TOTAL}$ psi	$\tilde{p}_{FILTERED} / \tilde{p}_{TOTAL}$	$\tilde{p}_{FILTERED}$ psi	$\tilde{p}_{FILTERED} / \frac{1}{2}\rho_\infty U_\infty^2$	$\tilde{p}_{TOTAL}$ psi	$\tilde{p}_{FILTERED} / \tilde{p}_{TOTAL}$
0	0.015	0.016	0.033	0.455	0.038	0.026	0.064	0.590	0.053	0.025	0.107	0.500	0.071	0.026	0.163	0.437
2	0.025	0.027	0.035	0.717	0.053	0.037	0.072	0.741	0.076	0.035	0.113	0.666	0.090	0.033	0.160	0.560
4	0.024	0.026	0.33	0.732	0.040	0.027	0.068	0.586	0.076	0.035	0.115	0.657	0.107	0.039	0.171	0.624
6	0.012	0.013	0.028	0.431	0.042	0.029	0.061	0.691	0.064	0.029	0.113	0.561	0.127	0.046	0.176	0.719
10	0.006	0.006	0.025	0.225	0.024	0.016	0.047	0.513	0.050	0.023	0.087	0.583	0.085	0.031	0.144	0.587
-2	0.013	0.014	0.035	0.381	0.028	0.019	0.064	0.442	0.038	0.018	0.100	0.379	0.071	0.026	0.155	0.460
-4	0.007	0.008	0.045	0.157	0.017	0.012	0.078	0.218	0.024	0.011	0.120	0.199	0.053	0.019	0.175	0.305
-6	0.008	0.008	0.060	0.125	0.011	0.008	0.096	0.118	0.016	0.007	0.145	0.110	0.045	0.016	0.203	0.221
-10	0.014	0.015	0.032	0.443	0.018	0.012	0.160	0.112	0.011	0.005	0.219	0.049	0.027	0.010	0.270	0.099

TABLE 15
EFFECT OF ANGLE OF ATTACK ON PRESSURE
OSCILLATIONS INSIDE CAVITY

WIDTH, b = 0.475 in.

DEPTH, d = 0.225 in.

LOCATION, ϕ = 60°

Angle of attack, α°	U_∞ = 341 ft/s				U_∞ = 426 ft/s				U_∞ = 514 ft/s				U_∞ = 585 ft/s			
	$\tilde{p}_{FILTERED}$ psi	$\frac{\tilde{p}_{FILTERED}}{\frac{1}{2}\rho_\infty U_\infty^2}$	$\tilde{p}_{TOTAL}$ psi	$\frac{\tilde{p}_{FILTERED}}{\tilde{p}_{TOTAL}}$	$\tilde{p}_{FILTERED}$ psi	$\frac{\tilde{p}_{FILTERED}}{\frac{1}{2}\rho_\infty U_\infty^2}$	$\tilde{p}_{TOTAL}$ psi	$\frac{\tilde{p}_{FILTERED}}{\tilde{p}_{TOTAL}}$	$\tilde{p}_{FILTERED}$ psi	$\frac{\tilde{p}_{FILTERED}}{\frac{1}{2}\rho_\infty U_\infty^2}$	$\tilde{p}_{TOTAL}$ psi	$\frac{\tilde{p}_{FILTERED}}{\tilde{p}_{TOTAL}}$	$\tilde{p}_{FILTERED}$ psi	$\frac{\tilde{p}_{FILTERED}}{\frac{1}{2}\rho_\infty U_\infty^2}$	$\tilde{p}_{TOTAL}$ psi	$\frac{\tilde{p}_{FILTERED}}{\tilde{p}_{TOTAL}}$
0	0.014	0.015	0.033	0.429	0.034	0.023	0.068	0.497	0.053	0.025	0.109	0.490	0.071	0.026	0.166	0.430
2	0.021	0.023	0.035	0.612	0.045	0.031	0.068	0.657	0.050	0.023	0.109	0.465	0.071	0.026	0.160	0.445
4	0.016	0.017	0.030	0.524	0.033	0.026	0.064	0.590	0.060	0.028	0.116	0.517	0.080	0.029	0.161	0.495
6	0.009	0.010	0.028	0.317	0.034	0.023	0.057	0.590	0.053	0.025	0.111	0.481	0.107	0.039	0.164	0.652
10	0.005	0.006	0.031	0.172	0.018	0.012	0.051	0.353	0.034	0.016	0.086	0.392	0.064	0.023	0.134	0.475
-2	0.013	0.014	0.035	0.359	0.023	0.015	0.068	0.329	0.034	0.016	0.107	0.314	0.053	0.019	0.158	0.338
-4	0.006	0.006	0.045	0.134	0.020	0.014	0.078	0.259	0.024	0.011	0.120	0.199	0.053	0.019	0.174	0.308
-6	0.006	0.006	0.058	0.130	0.019	0.013	0.093	0.205	0.021	0.010	0.140	0.152	0.034	0.012	0.193	0.175
-10	0.010	0.011	0.106	0.095	0.015	0.010	0.152	0.099	0.024	0.011	0.211	0.113	0.030	0.011	0.257	0.117

TABLE 16
EFFECT OF ANGLE OF ATTACK ON PRESSURE
OSCILLATIONS INSIDE CAVITY

WIDTH, b = 0.475 in.

DEPTH, d = 0.225 in.

LOCATION, ϕ = 90°

Angle of attack, α°	U_∞ = 341 ft/s				U_∞ = 426 ft/s				U_∞ = 514 ft/s				U_∞ = 585 ft/s			
	$\tilde{p}_{FILTERED}$ psi	$\tilde{p}_{FILTERED} / \frac{1}{2}\rho_\infty U_\infty^2$	$\tilde{p}_{TOTAL}$ psi	$\tilde{p}_{FILTERED} / \tilde{p}_{TOTAL}$	$\tilde{p}_{FILTERED}$ psi	$\tilde{p}_{FILTERED} / \frac{1}{2}\rho_\infty U_\infty^2$	$\tilde{p}_{TOTAL}$ psi	$\tilde{p}_{FILTERED} / \tilde{p}_{TOTAL}$	$\tilde{p}_{FILTERED}$ psi	$\tilde{p}_{FILTERED} / \frac{1}{2}\rho_\infty U_\infty^2$	$\tilde{p}_{TOTAL}$ psi	$\tilde{p}_{FILTERED} / \tilde{p}_{TOTAL}$	$\tilde{p}_{FILTERED}$ psi	$\tilde{p}_{FILTERED} / \frac{1}{2}\rho_\infty U_\infty^2$	$\tilde{p}_{TOTAL}$ psi	$\tilde{p}_{FILTERED} / \tilde{p}_{TOTAL}$
0	0.010	0.010	0.024	0.395	0.034	0.023	0.060	0.558	0.048	0.022	0.101	0.472	0.085	0.031	0.155	0.547
2	0.013	0.014	0.026	0.484	0.032	0.022	0.059	0.542	0.038	0.018	0.097	0.389	0.057	0.021	0.141	0.401
4	0.007	0.008	0.026	0.278	0.027	0.018	0.051	0.528	0.034	0.016	0.087	0.389	0.050	0.018	0.132	0.384
6	0.005	0.006	0.030	0.179	0.014	0.010	0.052	0.272	0.030	0.014	0.087	0.345	0.040	0.015	0.127	0.315
10	0.006	0.007	0.058	0.109	0.010	0.007	0.086	0.118	0.020	0.009	0.128	0.157	0.023	0.008	0.170	0.133
-2	0.011	0.012	0.025	0.450	0.023	0.015	0.055	0.409	0.030	0.014	0.096	0.312	0.053	0.019	0.144	0.370
-4	0.007	0.007	0.026	0.262	0.014	0.010	0.050	0.286	0.027	0.012	0.086	0.313	0.042	0.015	0.135	0.315
-6	0.005	0.906	0.031	0.172	0.011	0.007	0.055	0.194	0.018	0.008	0.088	0.204	0.032	0.012	0.134	0.238
-10	0.006	0.006	0.065	0.093	0.012	0.008	0.100	0.120	0.016	0.007	0.144	0.111	0.023	0.008	0.193	0.117

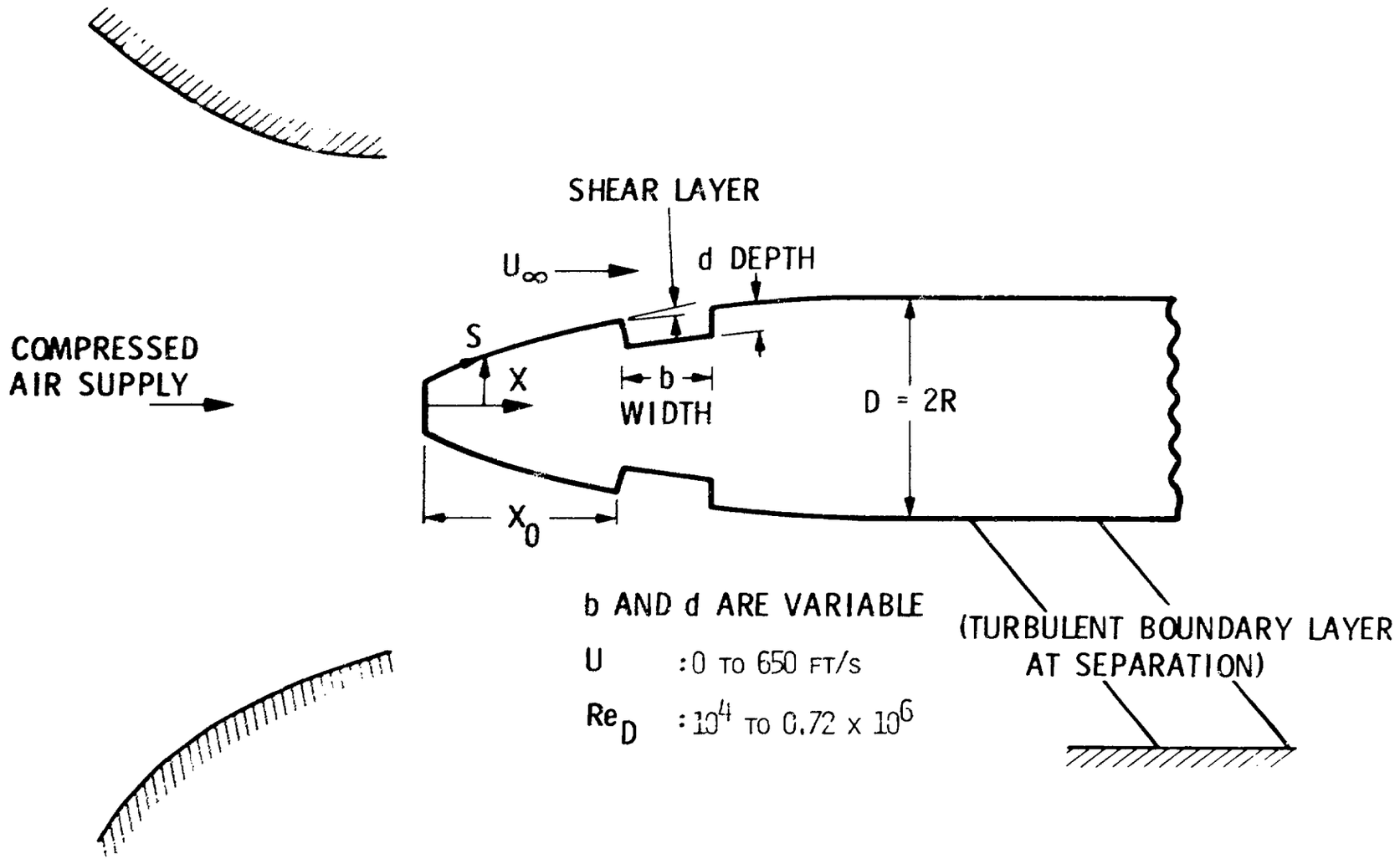

FIGURE 1. CAVITY OSCILLATION MODEL WITH PERTINENT NOMENCLATURE

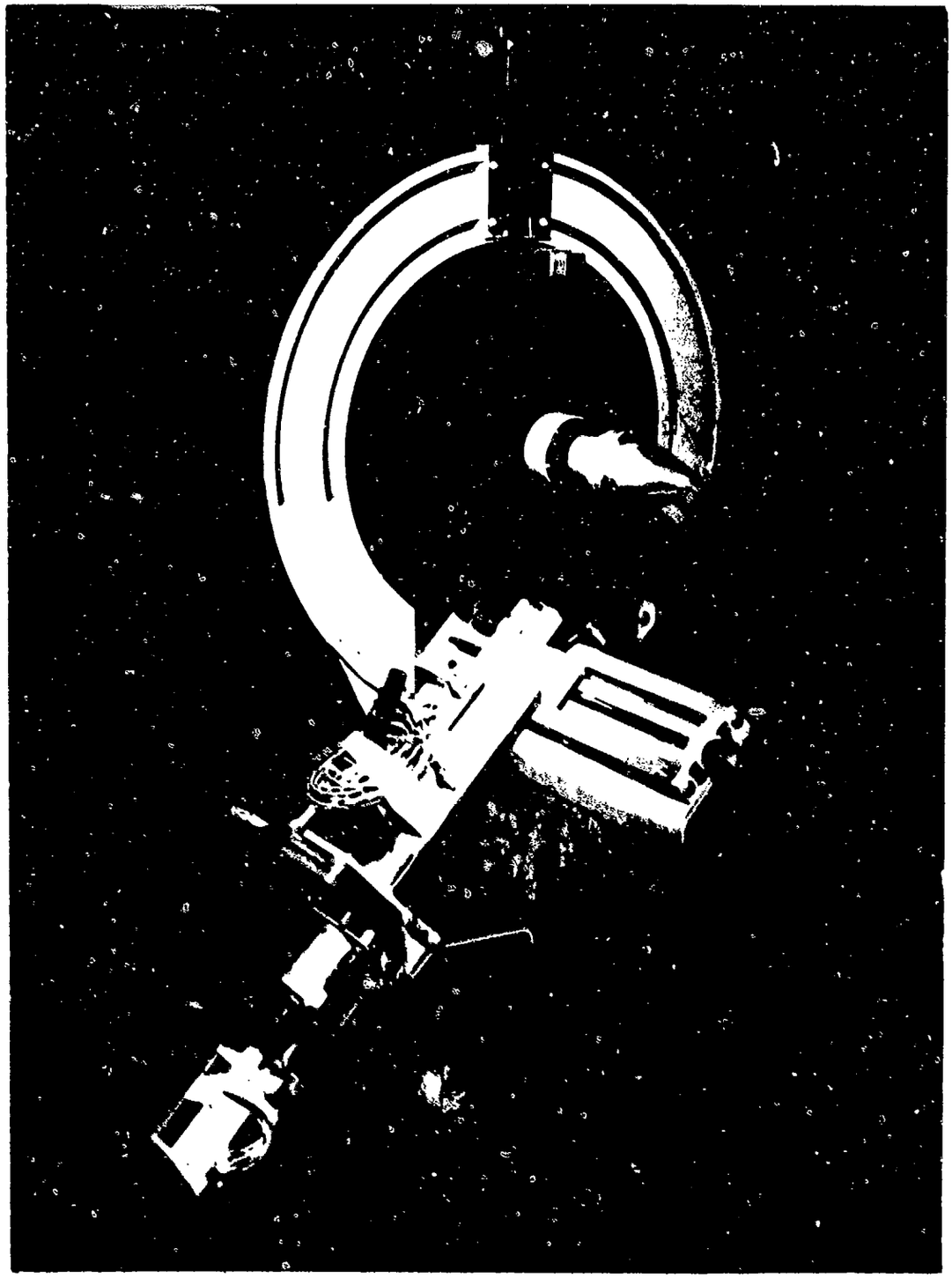

FIGURE 2. AXISYMMETRIC CAVITY FLOW SYSTEM

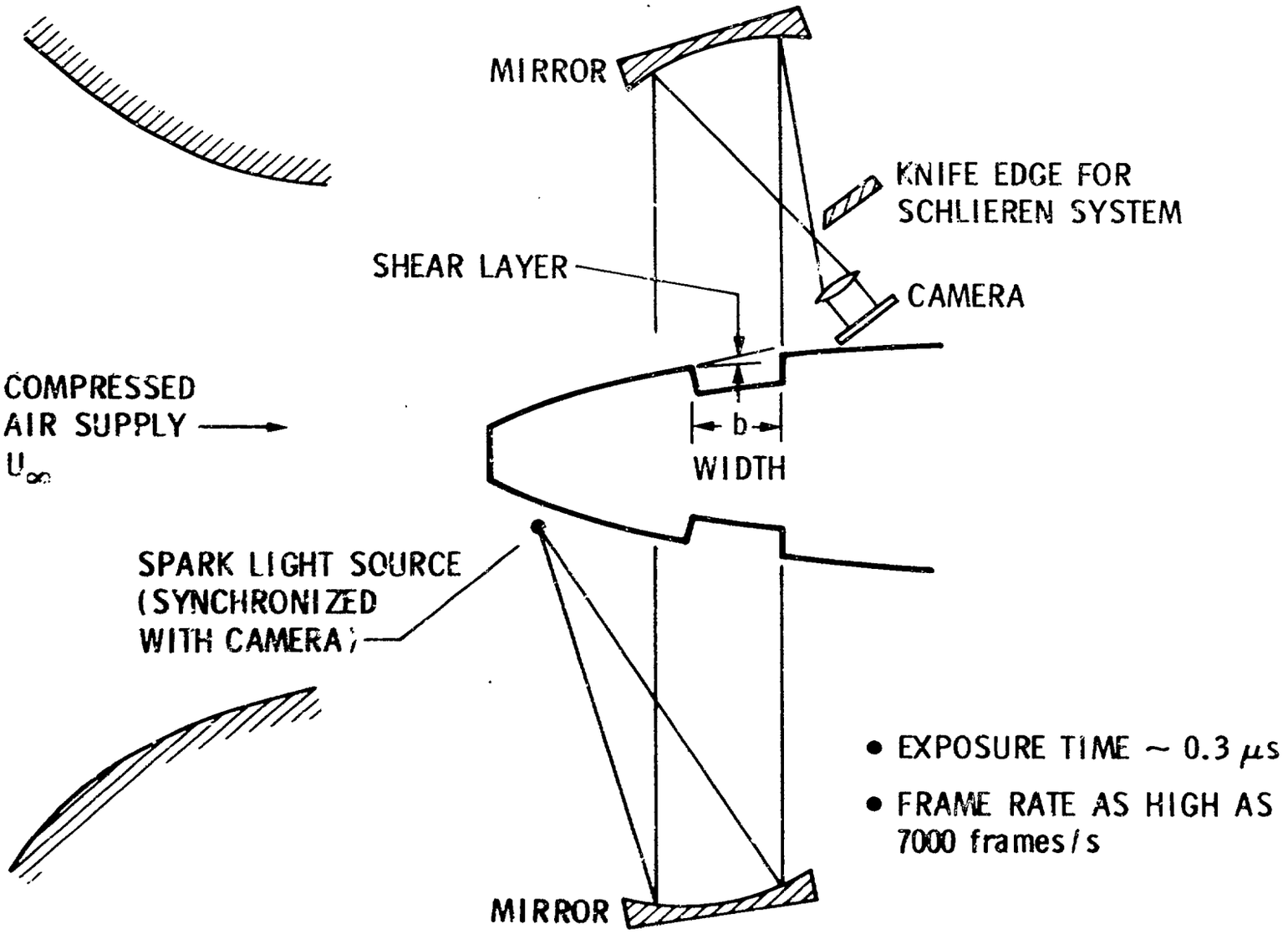

FIGURE 3. DIAGNOSTICS OF CAVITY FLOW OSCILLATIONS

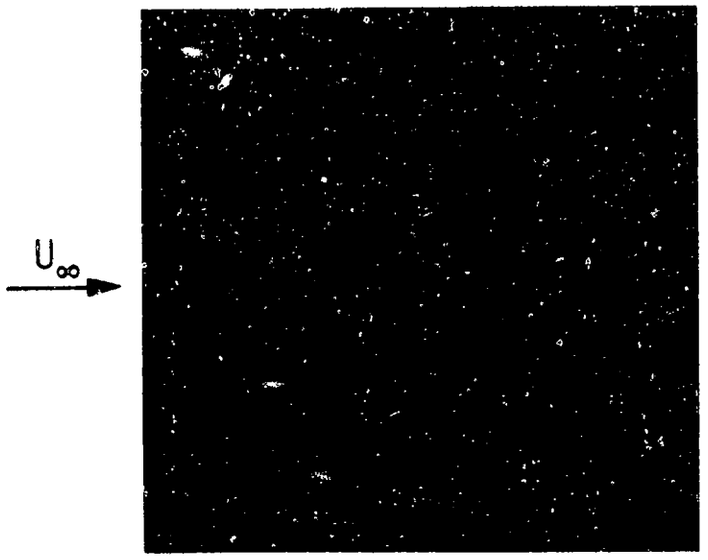

a) ANGLE OF ATTACK $\alpha = 0°$

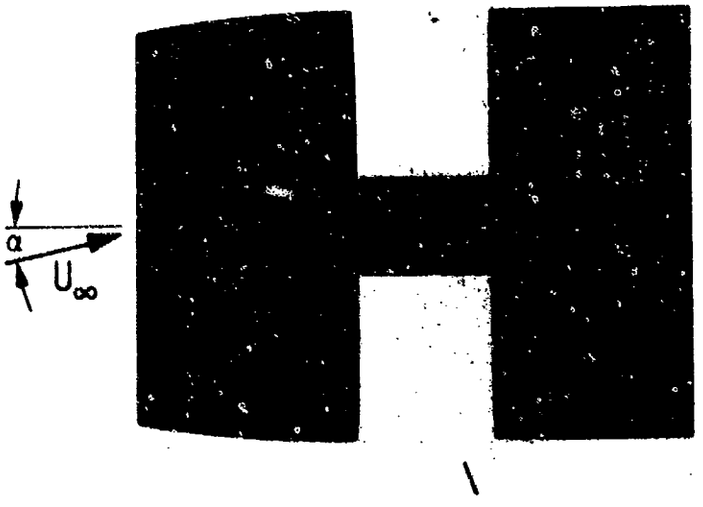

b) ANGLE OF ATTACK $\alpha = +4°$

FIGURE 4. VISUALIZATION OF CAVITY FLOW WITH b = 0.68 in., d = 0.75 in., and U_∞ = 60 ft/s

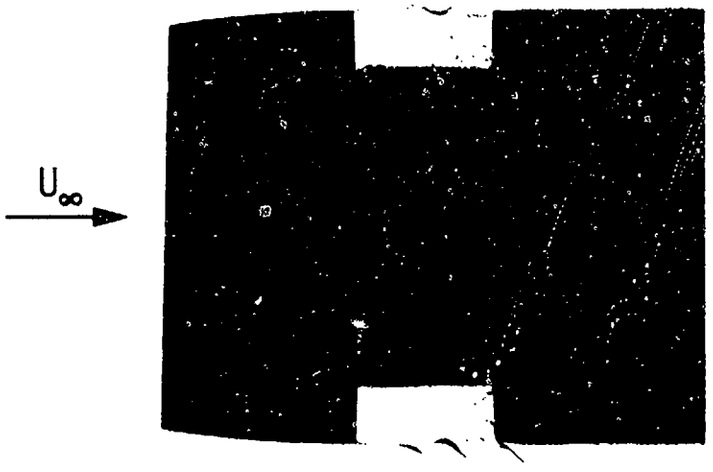

a) ANGLE OF ATTACK $\alpha = 0°$

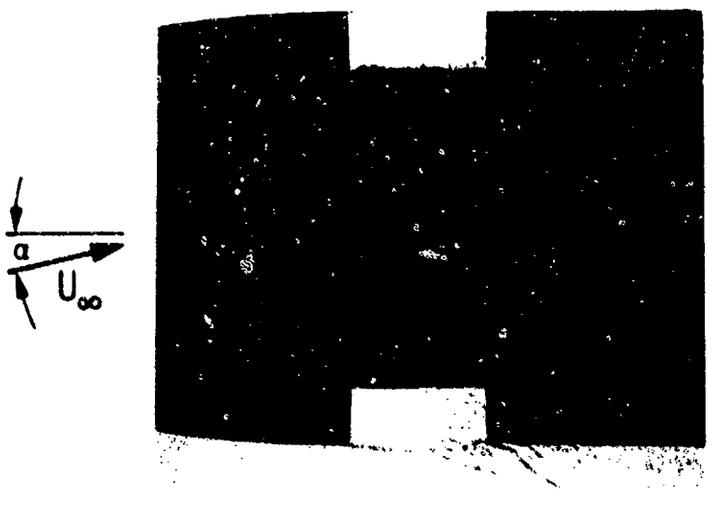

b) ANGLE OF ATTACK $\alpha = +4°$

FIGURE 5. VISUALIZATION OF CAVITY FLOW WITH b = 0.68 in., d = 0.25 in., and U_∞ = 60 ft/s

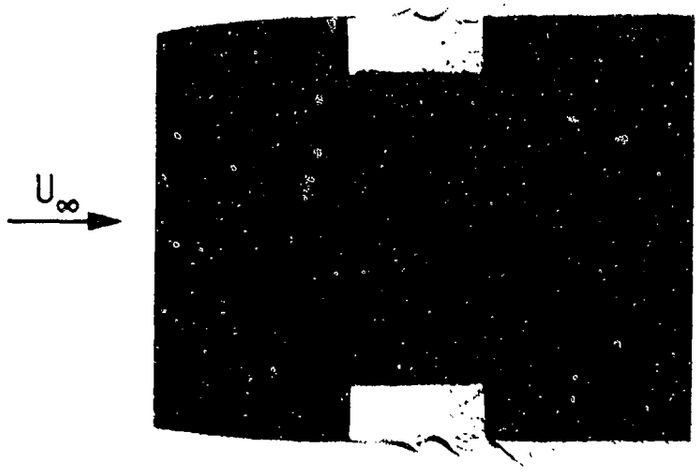

a) ANGLE OF ATTACK $\alpha = 0°$

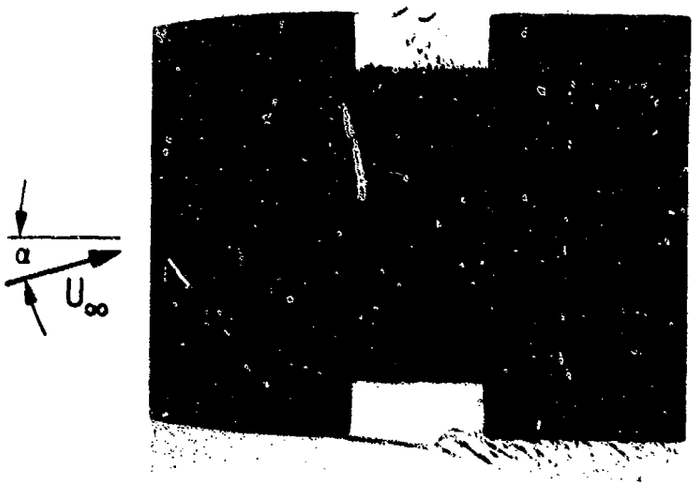

b) ANGLE OF ATTACK $\alpha = +6°$

FIGURE 6. VISUALIZATION OF CAVITY FLOW WITH b = 0.68 in., d = 0.25 in., and U_∞ = 60 ft/s

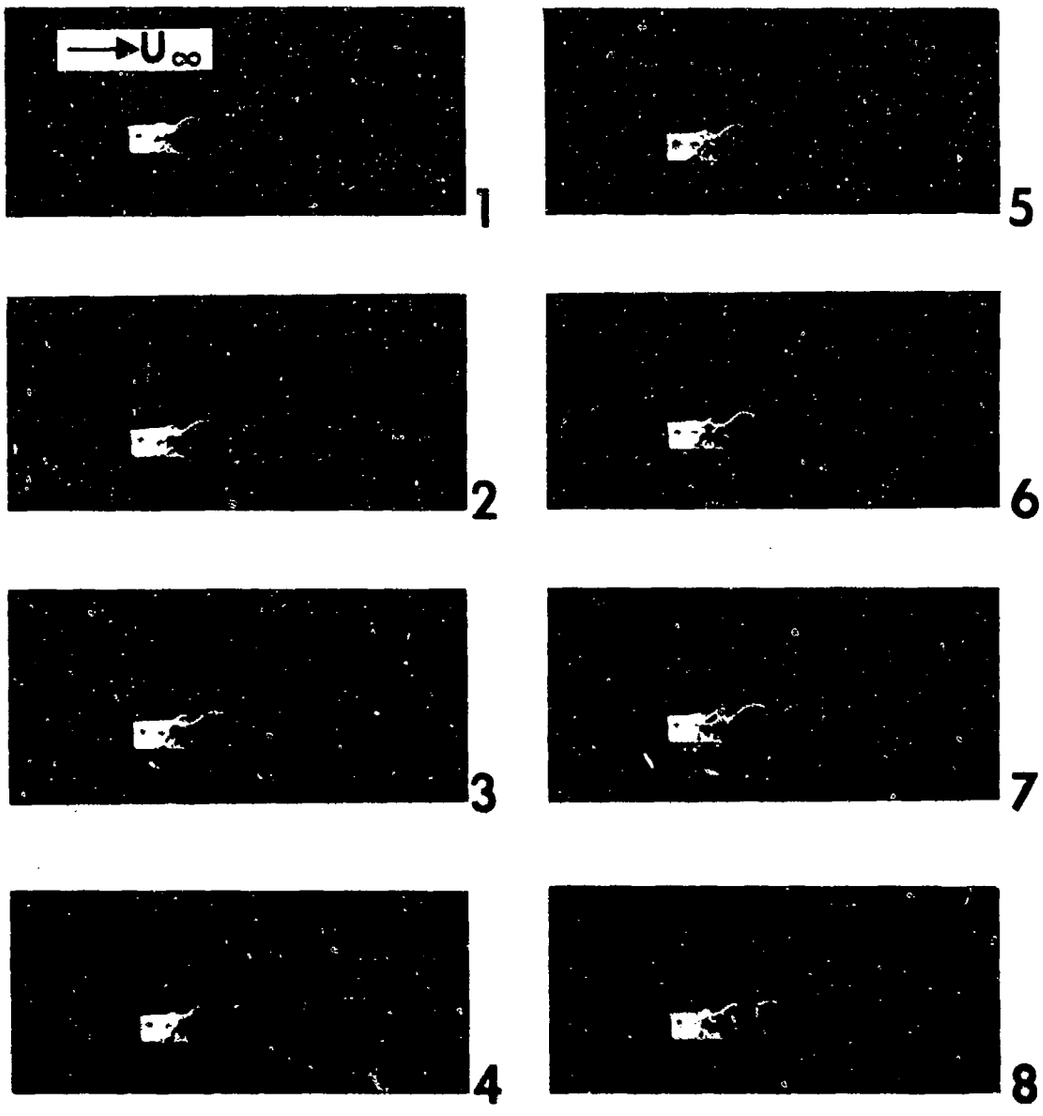

FIGURE 7. HIGH-SPEED SCHLIEREN MOTION PICTURES SHOWING LARGE-SCALE STRUCTURES IN OSCILLATING CAVITY FLOW AT α = 0° with U_∞ = 60 ft/s, b = 0.68 in., AND d = 0.25 in. (TIME BETWEEN FRAMES = 0.2 ms.)

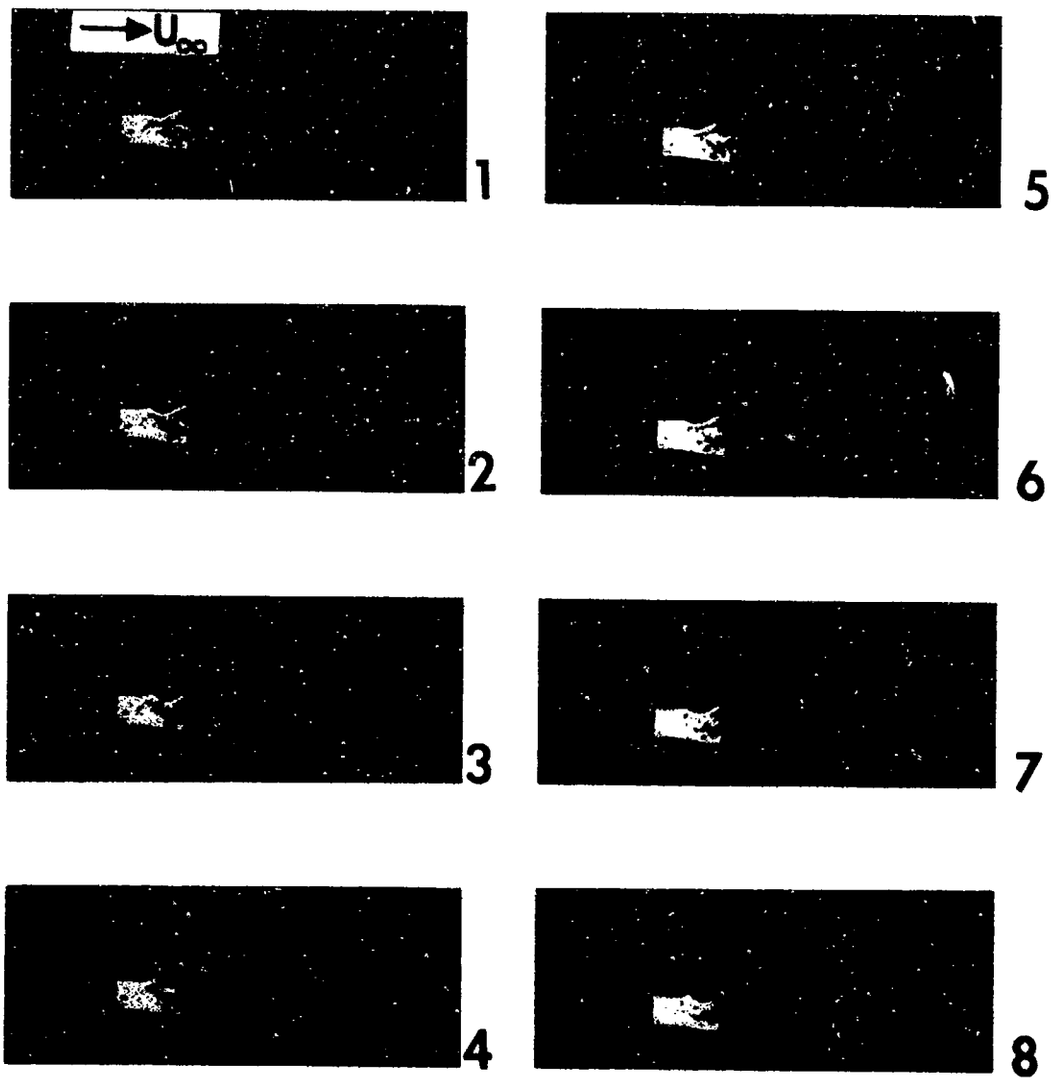

FIGURE 8. HIGH-SPEED SCHLIEREN MOTION PICTURES SHOWING LARGE-SCALE STRUCTURES IN OSCILLATING CAVITY FLOW AT α = 3.5° with U_∞ = 60 ft/s, b = 0.68 in., AND d = 0.25 in. (TIME BETWEEN FRAMES = 0.18 ms.)

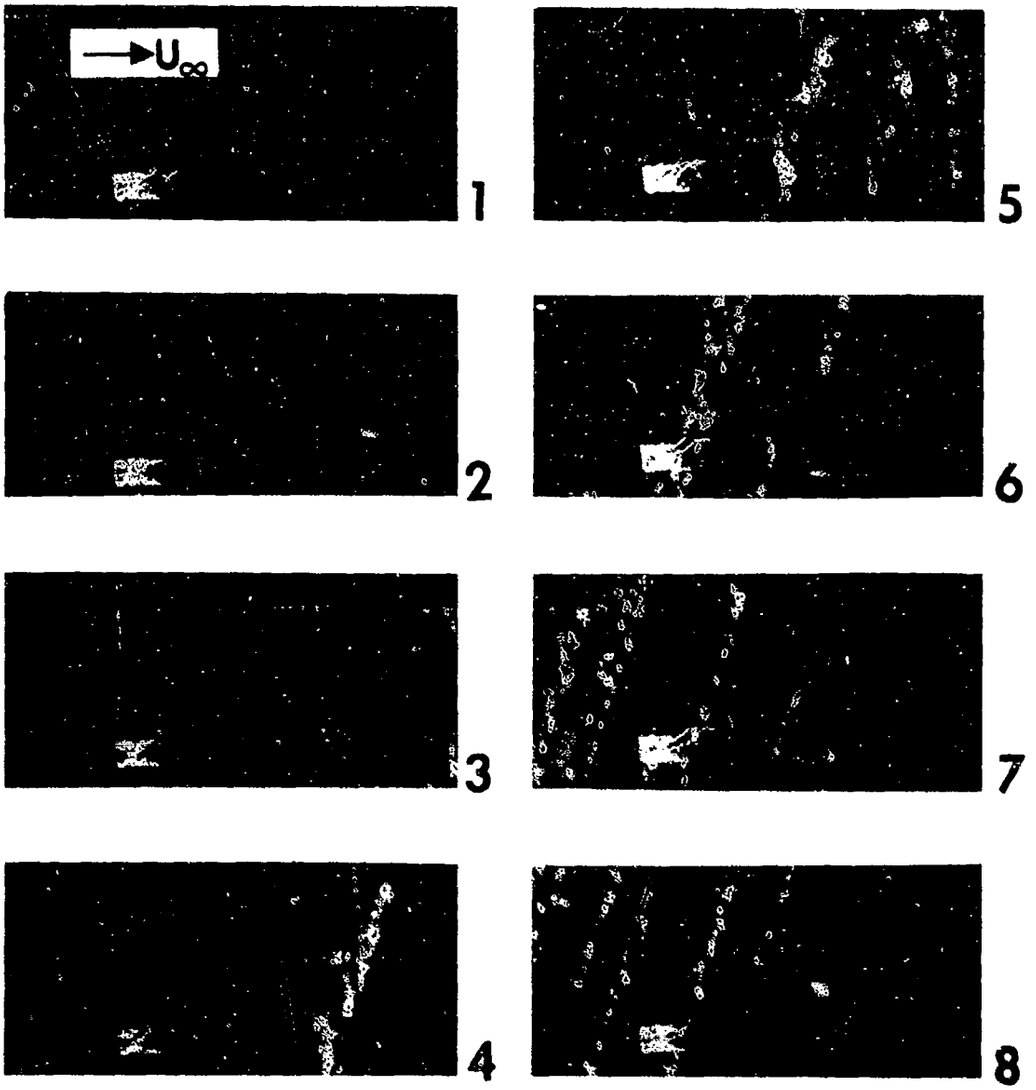

FIGURE 9. HIGH-SPEED SCHLIEREN MOTION PICTURES SHOWING LARGE-SCALE STRUCTURES IN OSCILLATING CAVITY FLOW AT α = -3.5° U_∞ = 60 ft/s, b = 0.68 in., AND d = 0.25 in. (TIME BETWEEN FRAMES = 0.18 ms.)

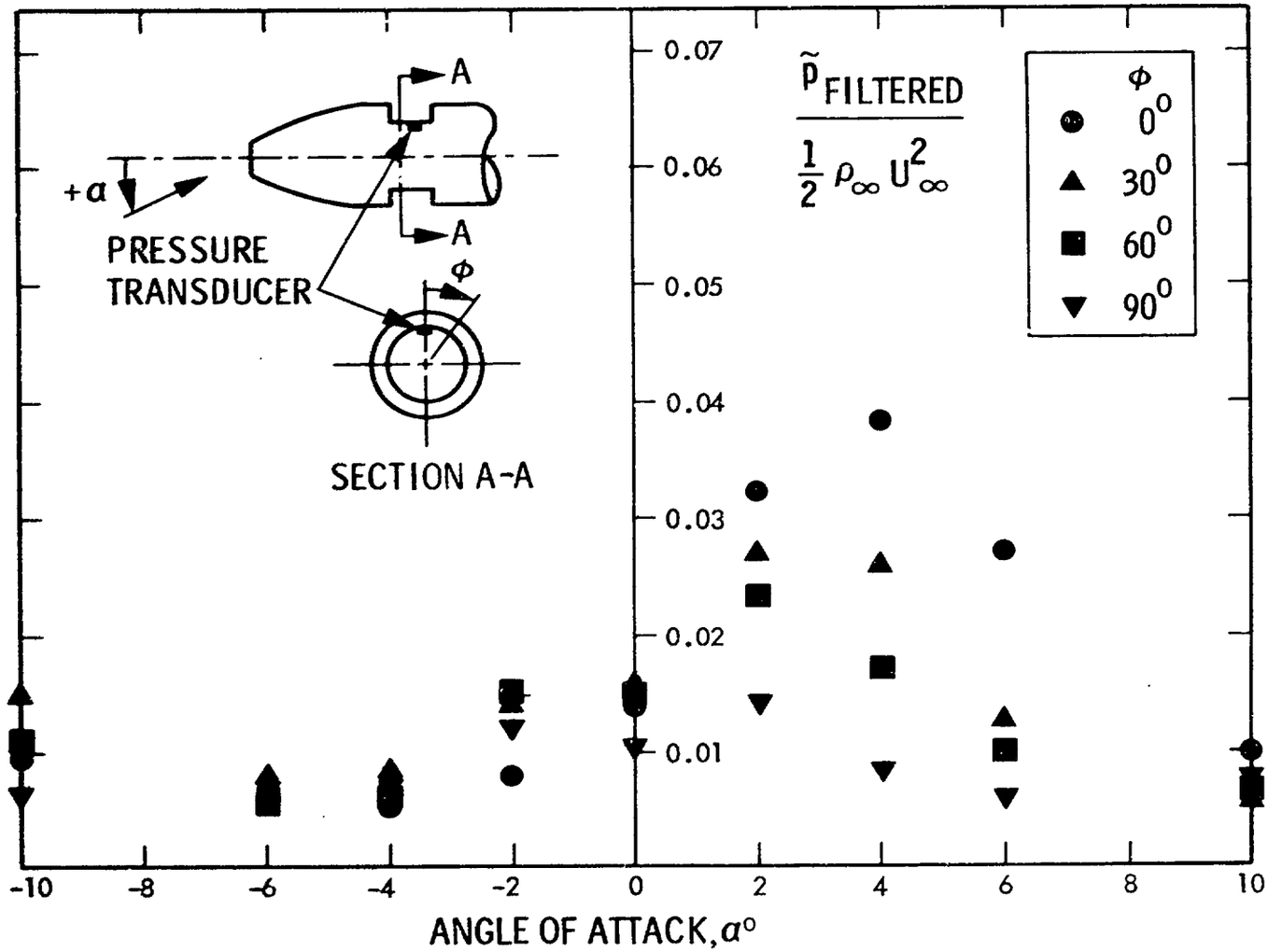

FIGURE 10. INFLUENCE OF ANGLE OF ATTACK ON CAVITY PRESSURE FLUCTUATIONS WITH b = 0.475 in., d = 0.225 in., and U_∞ = 341 ft/s

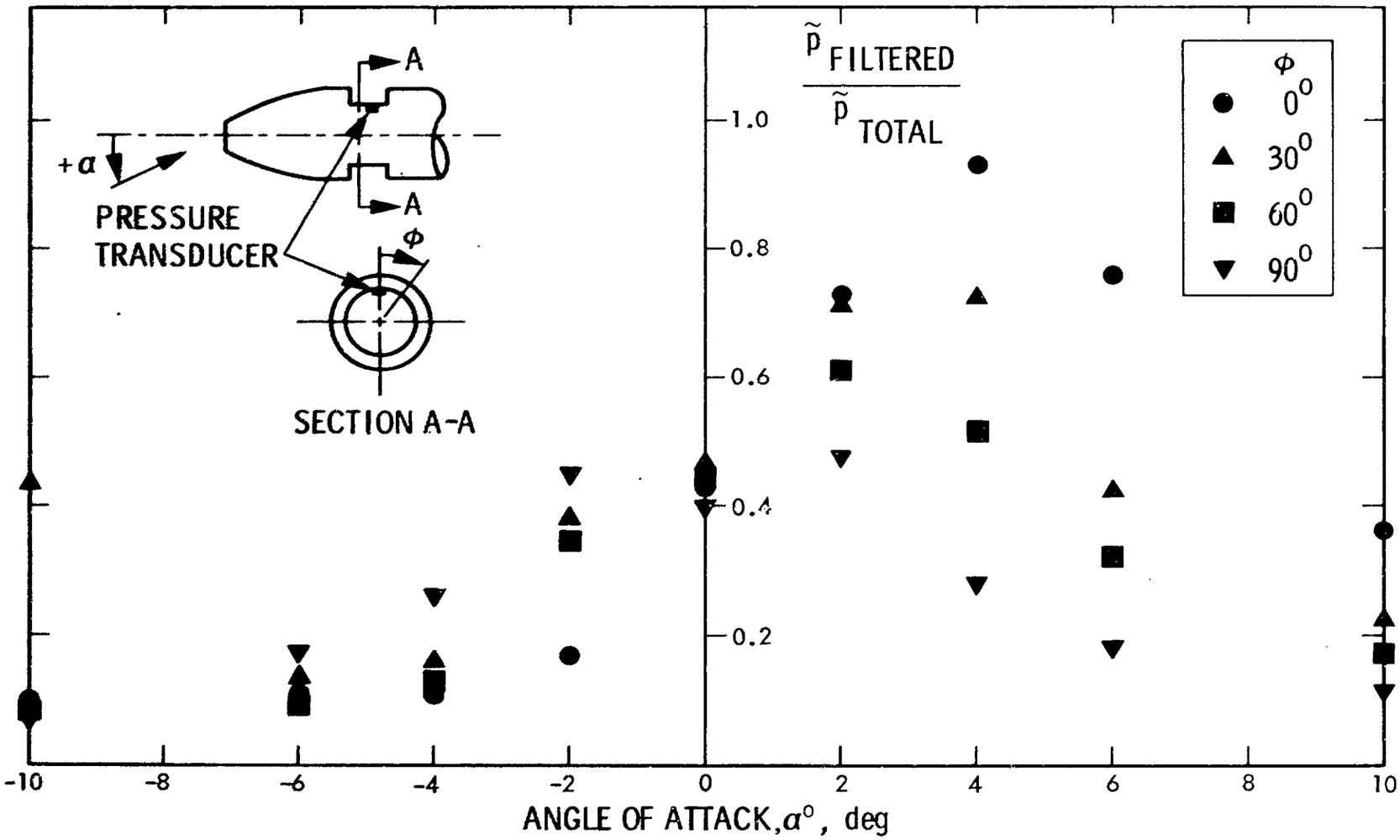

FIGURE 11. EFFECT OF ANGLE OF ATTACK ON CAVITY PRESSURE FLUCTUATIONS WITH b = 0.475 in., d = 0.225 in., and U_∞ = 341 ft/s

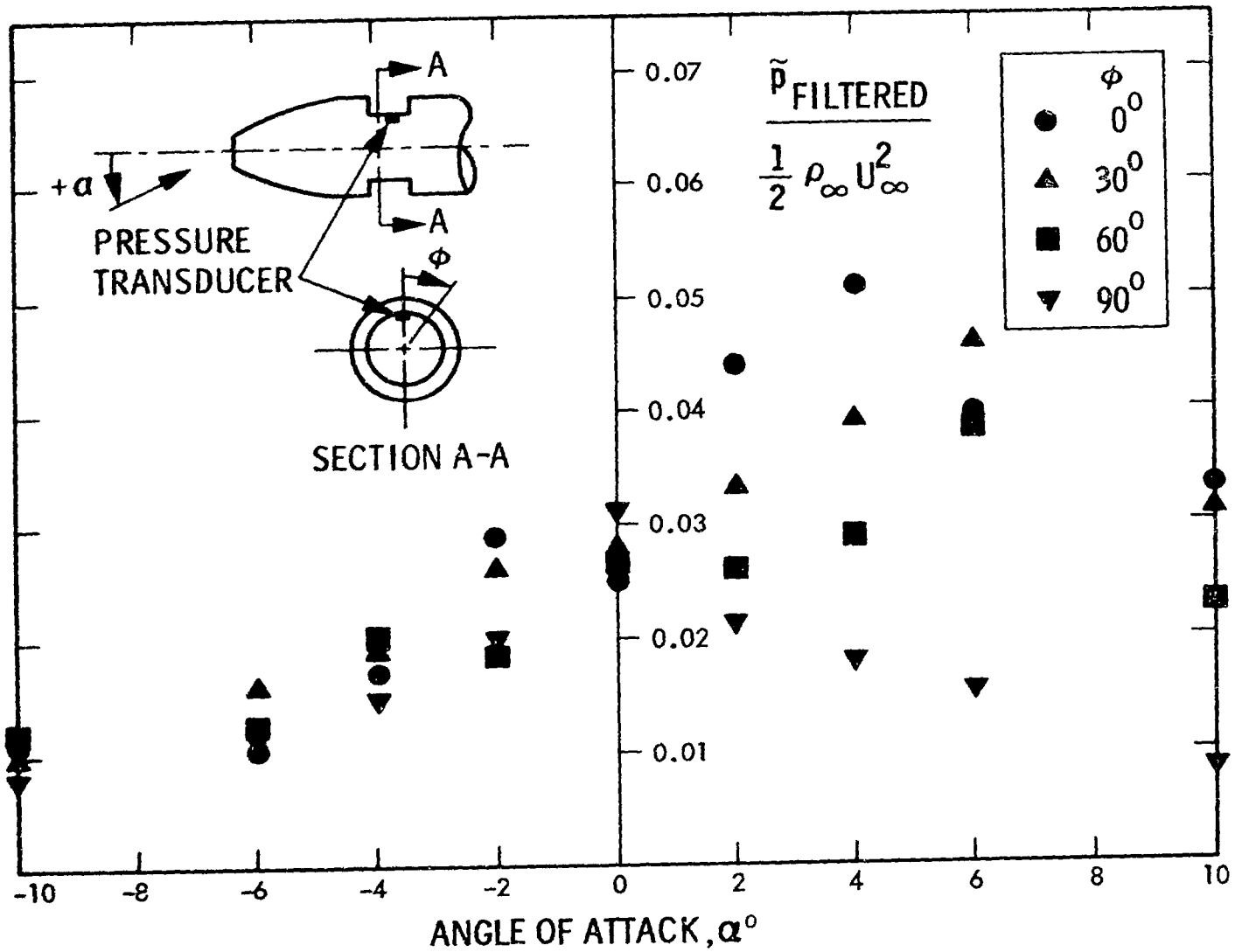

FIGURE 12. INFLUENCE OF ANGLE OF ATTACK ON CAVITY PRESSURE FLUCTUATIONS WITH b = 0.475 in., d = 0.225 in., and U_∞ = 585 ft/s

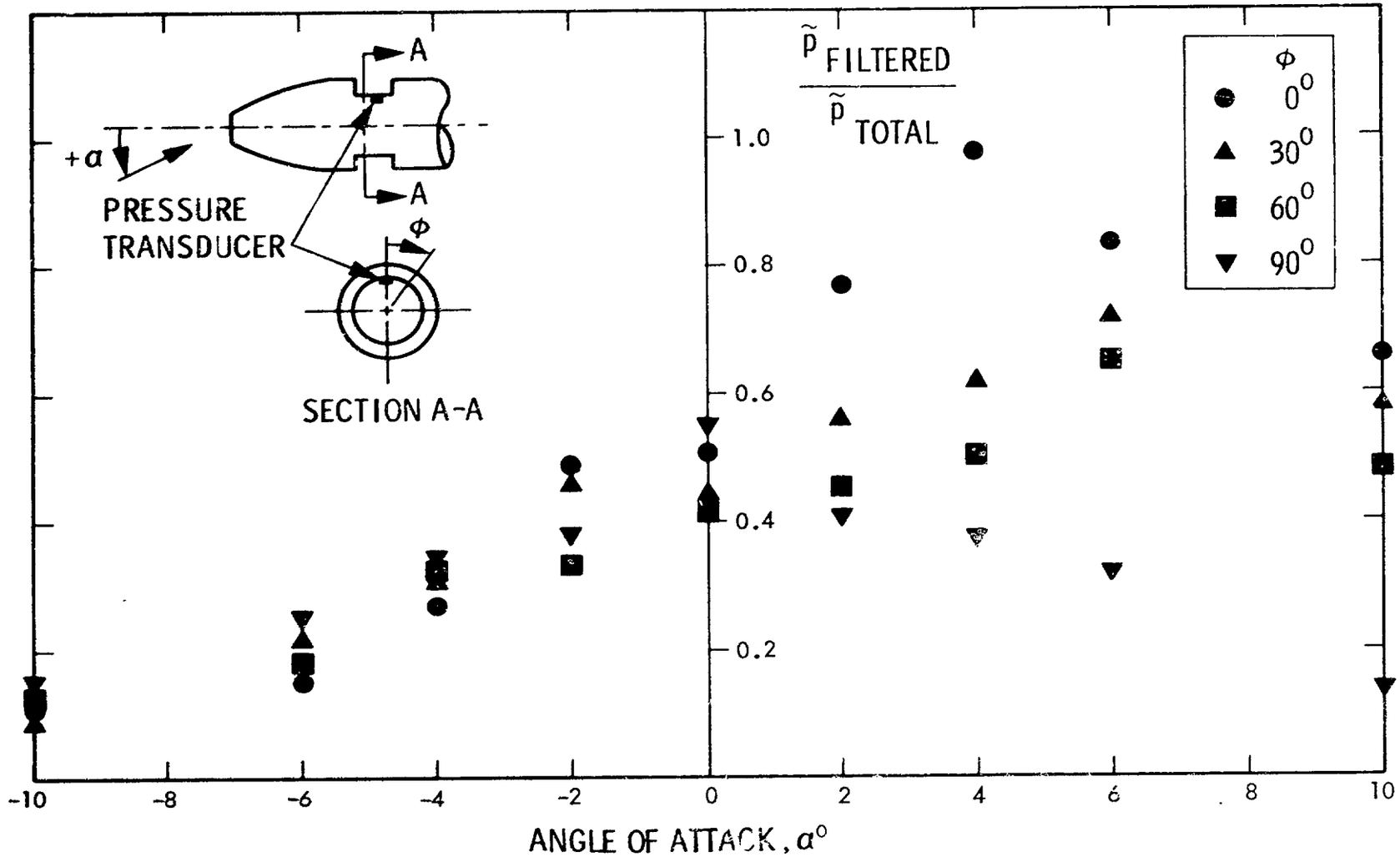

FIGURE 13. EFFECT OF ANGLE OF ATTACK ON CAVITY PRESSURE FLUCTUATIONS WITH b = 0.475 in., d = 0.225 in., and U_∞ = 585 ft/s

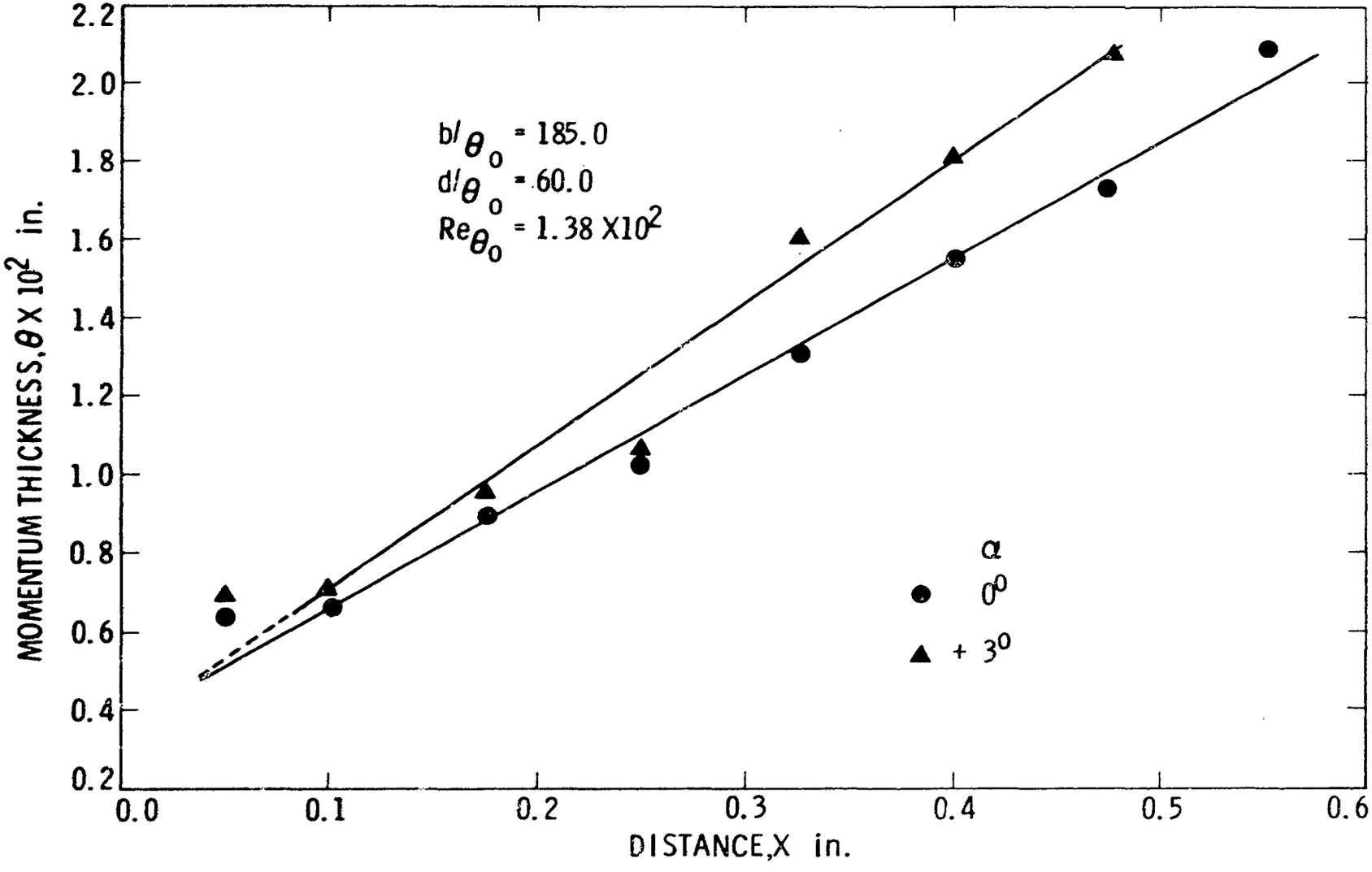

FIGURE 14. INFLUENCE OF ANGLE OF ATTACK ON SHEAR LAYER GROWTH RATE

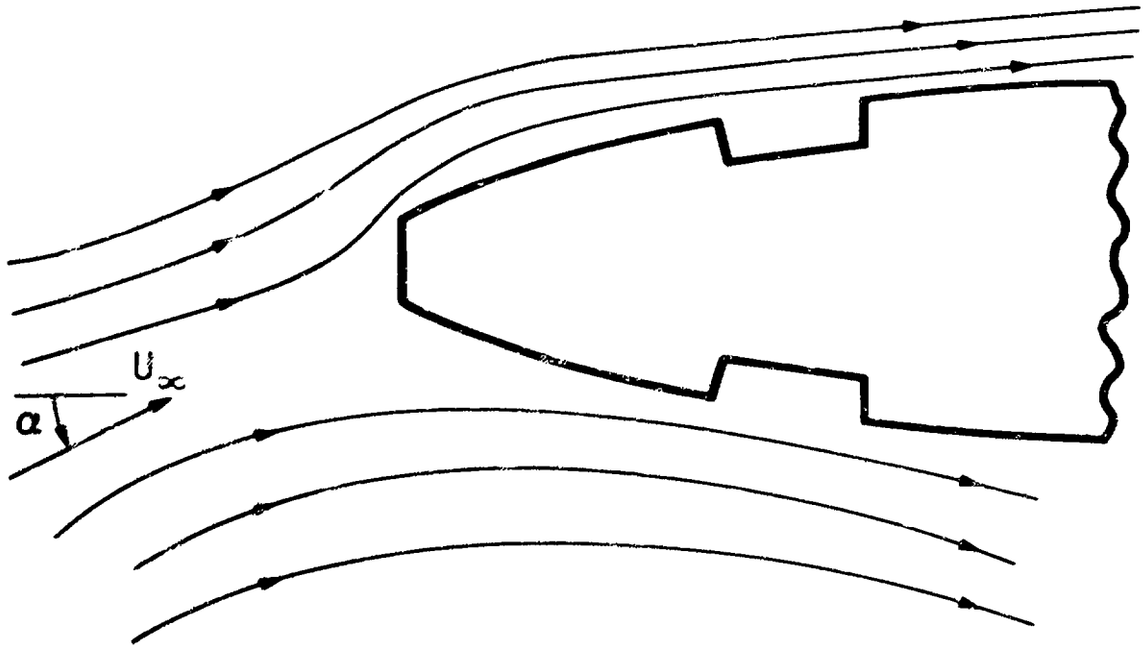

FIGURE 15. FLOW AROUND AXISYMMETRIC CAVITY AT ANGLE OF ATTACK

DISTRIBUTION LIST

Address

Defense Documentation Center, ATTN: DDC-TCA, Ca eron Station, Alexandria, Virginia 22314 (12 copies)

HDL Library, Harry Diamond Laboratories, 2800 Powder Mill Road, Adelphia, Maryland 20783 (3 copies)

Editorial Committee (Chairman), Harry Diamond Laboratories, 2800 Powder Mill Road, Adelphia, Maryland 20783

HDL Branch 013, Harry Diamond Laboratories, 2800 Powder Mill Road, Adelphia, Maryland 20783

HDL Branch 041, Harry Diamond Laboratories, 2800 Powder Mill Road, Adelphia, Maryland 20783

John Goto, Fluid Control Branch, Harry Diamond Laboratories, 2800 Powder Mill Road, Adelphia, Maryland 20783 (5 copies)

Richard Gottron, Fluid Control Branch, Harry Diamond Laboratories, 2800 Powder Mill Road, Adelphia, Maryland 20783

Lyndon J. Cox, Program and Plans Office, Harry Diamond Laboratories, 2800 Powder Mill Road, Adelphia, Maryland 20783

David L. Overman, S and A Devices, Branch 420, Harry Diamond Laboratories, 2800 Powder Mill Road, Adelphia, Maryland 20783

James K. O'Steen, Naval Surface Weapons Center, White Oak Laboratory, Silver Spring, Maryland 20910

Fred Sachs, U.S. Army Armaments Research and Development Command, Picatinny Arsenal, Dover, New Jersey 07801

James Murray, U.S. Army Research Office, P. O. Box 12211, Research Triangle Park, North Carolina 27709

Robert E. Singleton, Engineering Science Division, U.S. Army Research Office, P. O. Box 1211, Research Triangle Park, North Carolina 27709

D. Rockwell, Professor of Mechanical Engineering, Department of Mechanical Engineering and Mechanics, Lehigh University, Bethlehem, Pennsylvania 18015

California Institute of Technology, Graduate Aeronautical Laboratory, Pasadena, California 91109

M. V. Morkovin, Department of Mechanical and Aerospace Engineering, Illinois Institute of Technology, Chicago, Illinois 60619

A. Roshko, Mail Stop 205-50, Department of Aeronautics, California Institute of Technology, Pasadena, California 91125

Fazle Hussain, Director and Professor of Mechanical Engineering, Aerodynamics and Turbulence Laboratory, Cullen College of Engineering, Houston, Texas 77004

K. Karamcheti, Professor of Aeronautics, Department of Aeronautics and Astronautics, Stanford Univerisity, Stanford, California 94305

J. P. Woolley, Research Scientist, Nielsen Engineering & Research, Inc. 510 Clyde Avenue, Mountain View, California 94043